

Modulation of the Agulhas Current Retroflection and Leakage by Oceanic Current Interaction with the Atmosphere in Coupled Simulations

LIONEL RENAULT

Department of Atmospheric and Oceanic Sciences, University of California, Los Angeles, Los Angeles, California, and Laboratoire d'Étude en Géophysique et Océanographie Spatiale, IRD, Toulouse, France

JAMES C. MCWILLIAMS

Department of Atmospheric and Oceanic Sciences, University of California, Los Angeles, Los Angeles

PIERRICK PENVEN

Laboratoire d'Océanographie Physique et Spatiale, Université de Brest, CNRS, IRD, Ifremer, IUEM, Brest, France

(Manuscript received 19 July 2016, in final form 1 June 2017)

ABSTRACT


Coupled ocean–atmosphere simulations are carried out for the Mozambique Channel, the Agulhas Current system, and the Benguela upwelling system to assess the ocean surface current feedback to the atmosphere and its impact on the Agulhas Current (AC) retroflection and leakage. Consistent with previous studies, the authors show that the current feedback slows down the oceanic mean circulation and acts as an oceanic eddy killer by modulating the energy transfer between the atmosphere and the ocean, reducing by 25% the mesoscale energy and inducing a pathway of energy transfer from the ocean to the atmosphere. The current feedback, by dampening the eddy kinetic energy (EKE), shifts westward the distribution of the AC retroflection location, reducing the presence of eastern retroflections in the simulations and improving the realism of the AC simulation. By modulating the EKE, the AC retroflection and the Good Hope jet intensity, the current feedback allows a larger AC leakage (by 21%), altering the water masses of the Benguela system. Additionally, the eddy shedding is shifted northward and the Agulhas rings propagate less far north in the Atlantic. The current–wind coupling coefficient s_w is not spatially constant: a deeper marine boundary layer induces a weaker s_w . Finally the results indicate that the submesoscale currents may also be weakened by the current feedback.

1. Introduction

The Agulhas Current (AC) is the western boundary current of the south Indian Ocean Subtropical Gyre (e.g., Lutjeharms 2006), and it is known to have a strong influence on the climate and transports of heat and salt from the Indian Ocean to the Atlantic Ocean and the Southern Ocean. The sources of the AC are from the Mozambique Channel and from south of Madagascar; it flows along the southeastern coasts of Africa, transporting about 77 Sv ($1 \text{ Sv} = 1 \times 10^6 \text{ m}^3 \text{ s}^{-1}$; Beal et al.

2015) toward the south in a narrow band about 50 km wide with velocities often above 2 m s^{-1} (e.g., Boebel et al. 1998; Lutjeharms 2006). The AC is characterized by the presence of a retroflection at the south of the African continent, around 17°E , where the flow turns back on itself to return to the Indian Ocean (Lutjeharms and Van Ballegooyen 1988b).

The mesoscale activity in the Agulhas Basin region and the Mozambique Channel is among the largest of the world oceans (e.g., Ducet et al. 2000; Gordon 2003) and has a significant influence on the Atlantic Ocean, the Benguela upwelling system, and the global overturning circulation of the ocean (e.g., Gordon et al. 1987; de Ruijter et al. 1999a; Weijer et al. 1999; Biastoch et al. 2008b,a; McClean et al. 2011). AC water spreads into the South Atlantic, mainly through the AC leakage: Agulhas rings (large anticyclonic eddies) and eddies (e.g.,

 Denotes content that is immediately available upon publication as open access.

Corresponding author: Lionel Renault, lrenault@atmos.ucla.edu

Richardson 2007) shed at the Agulhas retroflection, transporting saltier and warmer water from the Indian Ocean. The transfer of Indian Ocean waters to the Atlantic via the AC retroflection is recognized as a key process for the closure of the thermohaline circulation (de Ruijter et al. 1999b; Beal et al. 2011). Paleooceanographic results and recent observations of a change in the Agulhas have stimulated active research on the subject (Zahn 2009; Beal et al. 2011). The AC leakage could strengthen the Atlantic meridional overturning circulation at a time when global warming and melting ice could slow it down (Beal et al. 2011). The AC leakage may also interact with the Benguela upwelling system and influence one of the most productive coastal environments of the world (Rae et al. 1992). Unlike the other eastern boundary upwelling systems (e.g., U.S. West Coast), much of the mesoscale activity of the Benguela is not generated along its coast through baroclinic and barotropic instabilities, rather it originates from the AC leakage (e.g., Matano and Beier 2003; Veitch et al. 2010). In simulations, a realistic AC and retroflection is therefore crucial in order to represent the AC leakage and thus the mesoscale variability and the water masses of the Benguela.

Because of the presence of Madagascar, the flow in the Mozambique Channel is dominated by eddies that propagate in the Agulhas Basin region and could affect the retroflection process (Schouten et al. 2002; Penven et al. 2006; Biastoch et al. 2008c; Rouault and Penven 2011). In particular, in the Natal Bight (29°S), the so-called Natal pulses (Harris et al. 1978; Lutjeharms and Van Ballegooyen 1988b; de Ruijter et al. 1999b), usually defined as large solitary meanders in the AC, are thought to play a significant role in determining the downstream variability of the AC and the subsequent leakage by the formation of Agulhas rings (Harris et al. 1978; Rouault and Penven 2011; Lutjeharms and Van Ballegooyen 1988b; van Leeuwen et al. 2000). Natal pulses may also cause the AC to short-cut its southwestern path for about 2–3 months, inducing a western or upstream AC retroflection (van Leeuwen et al. 2000). However, the numerical simulations of Biastoch et al. (2008c) do not show a significant influence of the Natal pulses on the AC leakage. Observations and numerical models have a wide range of AC leakage estimates between 2 and 18 Sv (de Ruijter et al. 1999a; Gordon 2003; Richardson 2007; van Sebille et al. 2009; Biastoch et al. 2008c,b,a; Putrasahan et al. 2015; Chen et al. 2016).

Although regional models can simulate some properties of the AC (Biastoch et al. 2008c; Loveday et al. 2014), the oceanic mesoscale turbulence in the region is difficult to model satisfactorily, for example, an AC retroflection farther east (upstream) and Agulhas rings

in a straight line in the South Atlantic (Lutjeharms and Webb 1995; Maltrud and McClean 2005; Barnier et al. 2006; Thoppil et al. 2011). With the exception of regional models where specific treatments are applied [e.g., large smoothing of the bathymetry or large value of diffusivity in Biastoch et al. (2008c) and Loveday et al. (2014)], a large majority of simulation models have persistent biases in representing the AC retroflection. Those issues persist even with high-resolution models (Thoppil et al. 2011).

The ocean has multiple feedbacks to the atmosphere. Recent studies using a coupled global model (e.g., Dawson et al. 2013) show the importance of resolving small-scale processes in the ocean to allow the atmosphere to be realistically forced. McClean et al. (2011), Putrasahan et al. (2016), Putrasahan et al. (2015), and Chen et al. (2016), using a high-resolution (0.1°) global coupled model, show that a coupled simulation allows a more realistic reproduction of the mean and mesoscale variability of the Agulhas system, both its leakage and eddy pathways compared to uncoupled oceanic simulations. In particular, various studies highlight the importance of the thermal feedback (e.g., Cornillon and Park 2001; Chelton et al. 2004; Park et al. 2006; Chelton et al. 2007; Spall 2007; Minobe et al. 2008), whereby the sea surface temperature (SST) can induce finescale structures in the wind. Chelton et al. (2004, 2007) derive linear relationships from satellite observations and numerical simulations between mesoscale SST and surface stress patterns. However, in the presence of strong SST gradients, other studies do not find such a linear relationship (e.g., Park et al. 2006; Liu et al. 2007). Small et al. (2008) is a review of the different processes involved. Another possible interaction between the ocean and the atmosphere is the current stress feedback. Although generally much weaker than the wind, the surface oceanic current can have an influence on the atmosphere. One of the main effects of the current feedback consists of a weakening of the mesoscale activity via a “mechanical dampening,” that is, a reduction of the work done by the wind on the ocean (wind work; Dewar and Flierl 1987; Duhaut and Straub 2006; Dawe and Thompson 2006; Eden and Dietze 2009; Seo et al. 2015; Renault et al. 2016d,c). However, Renault et al. (2016d) and Renault et al. (2016c) demonstrate using oceanic and atmospheric coupled simulations where a reduction of the mesoscale activity can be actually driven by a deflection of energy from the geostrophic current to the atmosphere. Renault et al. (2016d) show that the current feedback by reducing the surface induces a counteracting enhancement of the wind itself, which then partially reenergizes the ocean. Neglecting the current feedback when estimating the surface stress can also lead to an overestimation of the mean wind work and

the total energy of the ocean (Hughes and Wilson 2008; Scott and Xu 2009; Renault et al. 2016c). Consistent with Eden and Dietze (2009), Pacanowski (1987), and Luo et al. (2005), Renault et al. (2016c) shows that the current feedback slows down and stabilizes the Gulf Stream by reducing the input of energy from the atmosphere to the ocean and by dampening the mesoscale activity. Finally, McClean et al. (2011) show that a global, high-resolution, ocean–atmosphere, coupled simulation with thermal and mechanical coupling, improves the realism of the Agulhas rings, but they did not assess and explain the associated processes. The current feedback to the atmosphere may explain their results.

In this paper, we use a set of atmosphere–ocean coupled simulations and focus on the surface current feedback to the atmosphere. The objectives are to assess how the current feedback controls the AC characteristics and the air–sea energy flux and to address how it can modulate the AC retroflection and leakage. The paper is organized as follows: Section 2 describes the model configuration and methodology. In section 3, the direct effect of the current feedback on the mean and mesoscale circulation is assessed. In section 4, we show how the current feedback affects the AC retroflection and its leakage. Finally, the atmospheric response to the current feedback is assessed in section 5. The results are discussed and summarized in section 6.

2. Model configuration and methodology

a. The Regional Oceanic Modeling System

The oceanic simulations were performed with the Regional Oceanic Modeling System (ROMS; Shchepetkin and McWilliams 2005; Shchepetkin 2015) in its Coastal and Regional Ocean Community (CROCO) version. ROMS is a free-surface, terrain-following coordinate model with split-explicit time stepping and with Boussinesq and hydrostatic approximations. The grid covers the South African region, including the Mozambique Channel, Madagascar, the AC retroflection, and the Benguela, extending from 44.4° to 5.0°S and from 11.5°W to 50.0°E and is 1031×749 points with a spatial resolution between 4.5 and 6 km (4.8 km over the Agulhas Basin region). As in Loveday et al. (2014), although the southern boundary is relatively close to the Agulhas Current retroflection, it is far enough away to not interact with it (not shown). The model has a similar configuration to the one described by Renault et al. (2016c); it has 50 vertical levels. The vertical grid is stretched for increased boundary layer resolution using stretching surface and bottom parameters of $h_{\text{cline}} = 300$ m, $\theta_s = 7$, and $\theta_b = 2$. The domain is initialized using the Simple Ocean Data Assimilation (SODA)

climatological state of 1 January and spun up for 5.5 years using climatological monthly surface fluxes and lateral oceanic boundary conditions, reaching an equilibrium state. It is then run for an additional period, from June 1999 to 2004, using interannual, lateral, oceanic forcing as well as interannual surface forcing for all simulations. Temperature, salinity, surface elevation, and horizontal velocity initial and boundary information for the domain are taken from the monthly averaged SODA ocean interannual outputs (Carton and Giese 2008). Vertical mixing of tracers and momentum is done with a K-profile parameterization (KPP; Large et al. 1994). The diffusive part of the advection scheme is rotated along the isopycnal surfaces to avoid spurious diapycnal mixing (Lemarié et al. 2012). As in Penven et al. (2006) and Loveday et al. (2014), excess western boundary current variability is selectively damped via a horizontal viscosity parameterization A_h (Smagorinsky 1963):

$$A_h = 0.025 \times \frac{\Delta_x \Delta_y}{2} \times |\text{deformation tensor}|, \quad (1)$$

where Δ_x and Δ_y are the zonal and meridional scales. Only the period 2000–04 is analyzed.

b. The Weather Research and Forecast Model

The Weather Research and Forecast (WRF) Model (version 3.7.1; Skamarock et al. 2008) is implemented in a configuration with one grid. The Climate Forecast System Reanalysis (CFSR; ≈ 40 km spatial resolution; Saha et al. 2010) is used to initialize the model and to force it at the open boundary conditions from 1 June 1999 for 5.5 years. The domain has a horizontal resolution of 18 km and is slightly larger than the ROMS domain to avoid the effect of the WRF sponge (4 points). The parameterizations used here are similar to the one employed in Renault et al. (2016d); the reader is invited to refer to that study for more details. A bulk formula is used (Fairall et al. 2003) to estimate the freshwater, turbulent, and momentum fluxes provided to ROMS.

c. Experiments

The Ocean Atmosphere Sea Ice Soil, version 3.0 (OASIS3), coupler is used to exchange data fields every hours between ROMS and WRF (Valcke 2013). In the first experiment, named NOCURR, every hour WRF forces ROMS with the hourly averages of freshwater, heat, and momentum fluxes, whereas ROMS gives to WRF the hourly averaged SST. The surface stress is estimated with a quadratic form using the bulk formula described by Fairall et al. (2003):

$$\boldsymbol{\tau} = \rho_{\text{air}} C_D |\mathbf{U}| \mathbf{U}, \quad (2)$$

where $\boldsymbol{\tau}$ is the surface stress, ρ_{air} is the air density, C_D the surface drag coefficient, and \mathbf{U} the wind used to estimate the surface stress.

In NOCURR, the surface stress is computed using the absolute surface wind \mathbf{U}_a (at the first vertical level in WRF). The second experiment, CURR, is the very same experiment, but ROMS sends to WRF not only the SST but also the surface current \mathbf{U}_o (at the upper vertical level in ROMS). The surface stress is therefore estimated with a velocity that is the surface wind relative to the ocean surface current:

$$\mathbf{U} = \mathbf{U}_a - \mathbf{U}_o. \quad (3)$$

d. Energy budget

The numerical outputs for the solutions are daily averages. The mean ($\bar{}$) is defined with respect to long-term averaging (2000–04), and the prime denotes deviation from the long-term mean. The differences between the observations, CURR, and NOCURR, highlighted hereinafter, are significant at 95% according to a Student's t test.

Wind power to ageostrophic motions does not feed into the general circulation (e.g., Wunsch 1998; von Storch et al. 2007; Scott and Xu 2009). Then, as in, for example, Stern (1975) and Renault et al. (2016d), we focus on the following relevant source and eddy-mean conversion terms:

- geostrophic mean wind work

$$F_m K_{mg} = \frac{1}{\rho_0} (\overline{\tau_x u_{og}} + \overline{\tau_y v_{og}}), \quad (4)$$

where u_{og} and v_{og} are the zonal and meridional surface currents, τ_x and τ_y are the zonal and meridional surface stresses, and ρ_0 is mean seawater density;

- eddy geostrophic wind work

$$F_e K_{eg} = \frac{1}{\rho_0} (\overline{\tau'_x u'_{og}} + \overline{\tau'_y v'_{og}}); \quad (5)$$

- barotropic (Reynolds stress) conversion

$$K_m K_e = \int_z - \left(\overline{u'_o u'_o} \frac{\partial \overline{u_o}}{\partial x} + \overline{u'_o v'_o} \frac{\partial \overline{u_o}}{\partial y} + \overline{u'_o w'} \frac{\partial \overline{u_o}}{\partial z} \right. \\ \left. + \overline{v'_o u'_o} \frac{\partial \overline{v_o}}{\partial x} + \overline{v'_o v'_o} \frac{\partial \overline{v_o}}{\partial y} + \overline{v'_o w'} \frac{\partial \overline{v_o}}{\partial z} \right), \quad (6)$$

where w is the vertical velocity, and x , y , and z are the zonal, meridional, and vertical coordinates, respectively;

- and baroclinic conversion

$$P_e K_e = \int_z - \frac{g}{\rho_0} \overline{\rho' w'}, \quad (7)$$

where g is the gravitational acceleration.

The $F_m K_{mg}$ represents the transfer of energy from mean surface wind forcing to mean kinetic energy, $F_e K_{eg}$ represents the transfer of energy from surface wind forcing anomalies to geostrophic eddy kinetic energy (EKE), $K_m K_e$ represents the barotropic conversion from mean kinetic energy to EKE, and $P_e K_e$ represents the baroclinic conversion from eddy available potential energy to EKE. We computed those conversion terms at each model grid point. The wind work is estimated at the free surface, whereas the barotropic and baroclinic conversion terms are integrated over the whole water column. See Renault et al. (2016d,c) for more details. The current feedback induces a sink of energy on eddy time scale or longer time scales from the ocean geostrophic currents to the atmosphere. Although the current feedback effect on the geostrophic wind work and its consequences on the oceanic circulation is the main focus of this study, its effect on the ageostrophic motions (Ekman currents and submesoscale) is also discussed in section 3.

e. Position of the Agulhas retroflexion

As in Backeberg et al. (2012) and Loveday et al. (2014), the retroflexion extent is derived via a sea surface height (SSH) contour and tracked through the daily fields from AVISO and from the simulations. The contour value is determined from the mean SSH spanning 30°–32.5°S, 28°–32.5°E, capturing the upstream AC where the flow is less turbulent (see, e.g., Fig. 9d). To capture the inshore current edge, the mean value is considered where $200 < h < 1500$ m. The westernmost contour value is taken as the maximum loop extent (red dot in Fig. 9d).

f. Data

1) SURFACE STRESS FROM QUIKSCAT

The QuikSCAT-based Scatterometer Climatology of Ocean Winds (SCOW; Risien and Chelton 2008) is used to infer the mean surface stress. SCOW has a spatial resolution of 0.25°. The surface stress anomalies are derived from the QuikSCAT gridded product from Ifremer (Bentamy et al. 2013), which also has a spatial resolution of 0.25°.

2) AVISO ALTIMETRY

The daily absolute dynamic topography fields are obtained from the AVISO product (Ducet et al. 2000). The sea level anomaly data are based on a square grid of 0.25°, constructed by optimal interpolation in time and space

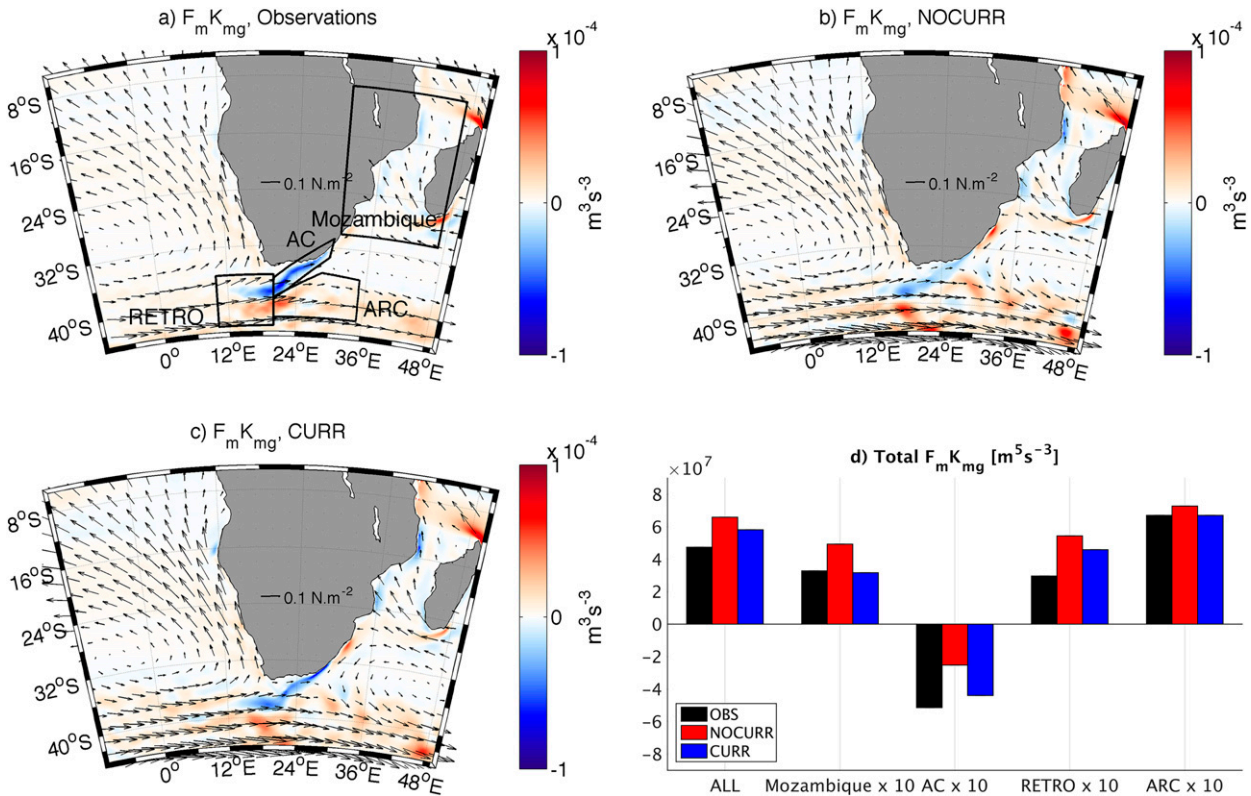


FIG. 1. Mean geostrophic wind work ($F_m K_{mg}$; color) and surface stress (vectors) estimated from (a) the observations, (b) NOCURR, and (c) CURR for the period 2000–04. (d) $F_m K_{mg}$ averaged over the whole domain (ALL), the regions over the Mozambique Channel (Mozambique), the AC, the Agulhas retroflection (Retro), and the ARC [see black boxes in (a)]. In (d) the Mozambique, AC, RETRO, and ARC values have been multiplied by a factor 10 to match the y scale. The current feedback to the atmosphere reduces $F_m K_{mg}$ by 12% over the whole domain.

from combined and intercalibrated altimeter missions using objective analysis (Le Traon et al. 1998). The daily absolute dynamic topography maps are then produced by adding the mean dynamic topographic data deduced from oceanic observations and an ocean general circulation model to the sea level anomaly (Rio et al. 2013).

3) TROPICAL RAINFALL MEASURING MISSION

The Tropical Rainfall Measuring Mission (TRMM) Multisatellite Precipitation Analysis, developed by the National Aeronautics and Space Administration (NASA) Goddard Space Flight Center (GSFC), provides a calibration-based sequential scheme for combining precipitation estimates from multiple satellites at fine spatial and temporal scales ($0.25^\circ \times 0.25^\circ$ and 3 hourly) over $50^\circ N$ – $50^\circ S$ (Huffman et al. 2007).

3. Current feedback impact on the circulation

a. Mean geostrophic circulation

The mean atmospheric surface circulation is fairly well represented in both NOCURR and CURR with respect to

the observations (see arrows in Fig. 1) and is characterized by the presence of the prevailing wind in the southern part of the domain and by the influence of the South Atlantic anticyclone, which induces equatorward surface winds along the Namibia and Angola coasts. The Mozambique Channel is characterized by a west-northward surface stress and by the presence of an anticyclonic circulation south of Madagascar. The mean biases of the zonal and meridional surface stress components are weak (not shown) and close to the associated error of the observations: 0.011 and $0.013 N m^{-2}$ (0.010 and $0.011 N m^{-2}$) for NOCURR (CURR) with respect to the SCOW estimates (Risien and Chelton 2008).

Figure 2 depicts the mean surface stress curl (colors) and the mean surface current vorticity (contours) from the observations (SCOW and AVISO) and the simulations. The presence of the AC has a very clear effect on the surface stress curl and on the surface current vorticity. A positive and negative surface stress curl along the AC arises in QuikSCAT and CURR but not in NOCURR (Fig. 2). This stress curl can have two origins: 1) the SST feedback to the atmosphere (present in both CURR and NOCURR) and 2) the direct effect of the surface

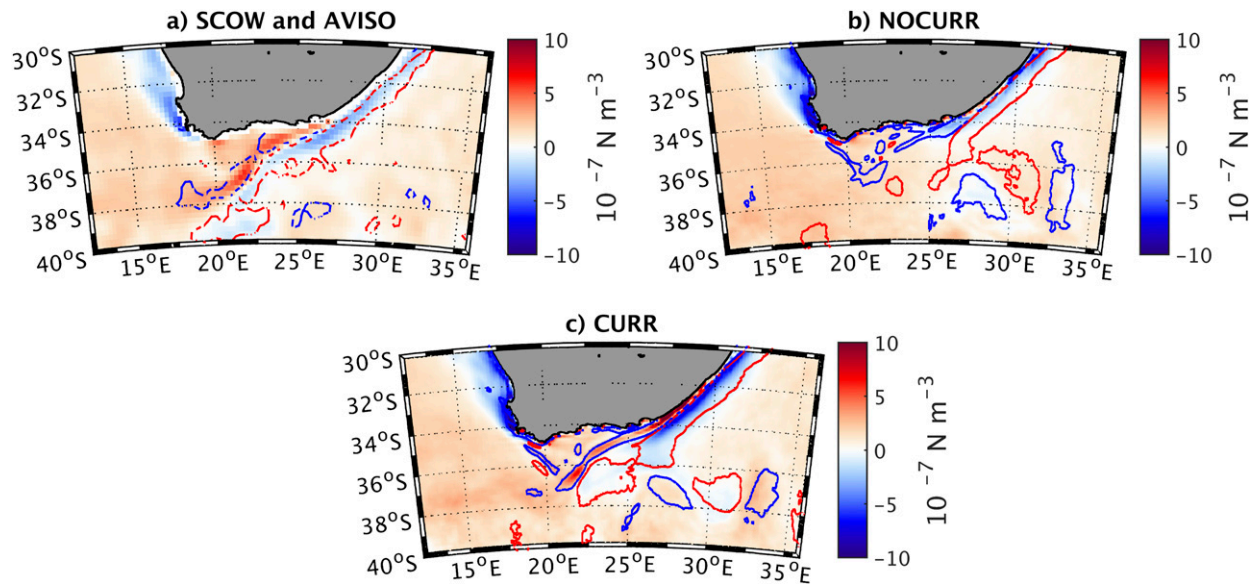


FIG. 2. Mean surface stress curl and surface current vorticity; the colors represent the mean surface stress curl from SCOW and from NOCURR and CURR for the period 2000–04. The blue (red) contour represents the mean negative (positive) vorticity of the geostrophic surface currents from AVISO and the simulations for the same period (only contours of $\pm 2 \times 10^{-6} \text{ m s}^{-1}$ for AVISO and $\pm 7 \times 10^{-6} \text{ m s}^{-1}$ for the simulations are shown for clarity). In the observations and in CURR, a negative (positive) surface current vorticity induces a positive (negative) surface stress curl.

current on the surface stress. [Small et al. \(2008\)](#) provide a review of the different mechanisms related to the SST feedback to the atmosphere. Here, as depicted in [Fig. 3](#), the wind curl in CURR and the difference in wind curl between CURR and NOCURR are clearly marked by the presence of the AC and have, thus, a very similar spatial pattern than the surface stress curl in CURR ([Fig. 3c](#)). In CURR, the wind has an opposite response to the surface stress (and does not correspond to weak changes in the marine boundary layer, as mentioned in [section 5](#)). When the mean currents are moving in the same (opposite) direction as the wind, the current feedback decreases (increases) the mean surface stress up to 0.2 N m^{-2} [$\tau = C_D \rho_a (\mathbf{U}_a - \mathbf{U}_o)^2 < C_D \rho_a (\mathbf{U}_a)^2$]. Less (more) surface stress induces less (more) surface friction and then allows the surface wind to accelerate (weaken). As a result, a positive surface current vorticity induces a negative surface stress curl, which in turn generates a positive wind curl. This is consistent with [Chelton et al. \(2004\)](#); over the Agulhas Basin, the strong mean surface currents (about 1 m s^{-1} for the AC) induce a positive and negative stress curl in QuikSCAT and in CURR but not in NOCURR. Scatterometers measure the actual surface stress that depends on the difference between wind and ocean velocities ([Chelton et al. 2004](#)). CURR, unlike NOCURR, estimates the surface stress using the difference between wind and ocean velocities. Note that the QuikSCAT wind product does not reproduce the wind

response to the stress changes induced by the current feedback because they are by definition a 10-m neutral wind estimated from the measured pseudostress without removing the current influence (not shown).

From an oceanic point of view, in CURR the AC surface current vorticity is better represented with respect to the observations because of a more realistic energy balance between the ocean and the atmosphere. The large values of negative surface stress curl along the African coast are mainly induced by the presence of the orography and coastline meandering ([Renault et al. 2016b](#); [Desbiolles et al. 2016](#)); they may be underestimated by the QuikSCAT products due to the contamination of the land and satellite coastal blind zone ([Renault et al. 2009](#)). From NOCURR to CURR, the current feedback improves the realism of the surface stress curl but also, as detailed hereafter, improves the realism of the mean oceanic circulation.

[Figure 1](#) depicts the $F_m K_{mg}$ as estimated from the observations (using AVISO and SCOW) and the simulations. As depicted in [Figs. 1a and 1d](#), five specific regions are considered: the whole domain, the Mozambique Channel, the AC, the AC retroflection, and the Agulhas Return Current (ARC). The $F_m K_{mg}$ is generally positive because the surface currents mainly flow in the same direction as the surface stress, but it also presents large negative values, where the mean AC flows in the opposite direction from the surface stress.

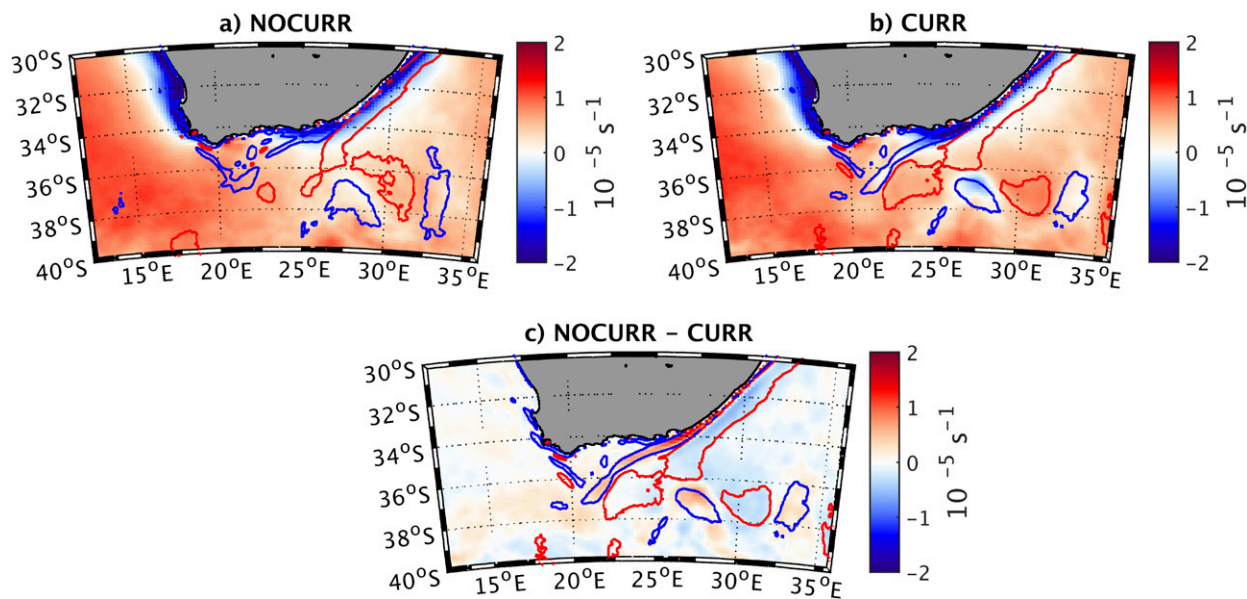


FIG. 3. (a),(b) Mean surface (first level in WRF) wind curl and surface current vorticity; the colors represent the mean surface wind curl from (a) NOCURR and (b) CURR for the period 2000–04. The blue (red) contour represents the mean negative (positive) vorticity of the geostrophic surface currents from the simulations for the same period (only contours of $\pm 7 \times 10^{-6} \text{ m s}^{-1}$ are shown for clarity). (c) Mean wind curl difference between NOCURR and CURR along with the current vorticity from CURR. The surface stress increase (decrease) in CURR induces a decrease (increase) of the surface wind in the simulation with current feedback.

This large deflection of energy from the ocean to the atmosphere is underestimated in NOCURR (by 50%) because it neglects the surface current when estimating the stress and therefore does not represent the positive surface stress curl collocated over the AC (Fig. 2). Overall, NOCURR overestimates $F_m K_{mg}$ with respect to the observations by 35% over the whole domain and in particular by 50%, 67%, and 10% over the Mozambique Channel, the AC retroflection, and the ARC. This could be partly due to the spatial resolution and smoothing used in AVISO; however, in CURR, when taking into account the surface current into the estimation of the surface stress, the $F_m K_{mg}$ biases are largely reduced. From NOCURR to CURR, $F_m K_{mg}$ is reduced by 12% over the whole domain. The main changes occur where the current is the largest, that is, along the Mozambique Channel, where $F_m K_{mg}$ is reduced by 20%, and over the AC, where $F_m K_{mg}$ is increased (negatively) by 74% (Fig. 1d). Over the AC retroflection and the ARC, $F_m K_{mg}$ is reduced by 18% and 8%. The $F_m K_{mg}$ improvement from NOCURR to CURR is partly explained by the surface stress changes but also as inferred after from an adjustment of the surface currents. The $F_m K_{mg}$ in CURR still has some biases with respect to the observations of 21% over the whole domain. While some of these are obviously due to model bias, there is a possible underestimation of the mean current in AVISO (Rio et al. 2011, 2013). Note that, locally, the wind has an

annual cycle that can change its direction, for example, near 34°S; the wind can blow toward the same direction as the surface current (positive $F_m K_{mg}$) or in the opposite direction as the surface current (negative $F_m K_{mg}$). In the case of wind blowing in the same direction as the surface current, the current feedback will reduce the surface stress and therefore the positive $F_m K_{mg}$. If it is blowing in the opposite direction, the current feedback reinforces the surface stress (i.e., it becomes more negative), increasing the deflection of energy from the ocean to the atmosphere (i.e., more negative $F_m K_{mg}$). In any event, from an energetic point of view, the effect of the current feedback is the same: it reduces the available energy of the ocean.

Figure 4 depicts the mean surface geostrophic currents from AVISO and from the simulations and the total depth-integrated kinetic energy (KE) evaluated over the whole domain and the same regions used for the $F_m K_{mg}$ analysis (black boxes in Fig. 1a). The mean surface geostrophic currents are better represented in CURR; the AC path is narrower, and the AC retroflection is more realistic (see section 4). In the observations and in CURR, at the surface, the AC reaches, on average, a maximum velocity of 1.1 m s^{-1} , whereas in NOCURR, due to a too persistent eastern retroflection (section 4), it reaches only 0.8 m s^{-1} . Consequently, the Good Hope jet reaches values of 0.4 m s^{-1} in CURR and in AVISO versus 0.3 m s^{-1} in NOCURR. This may alter

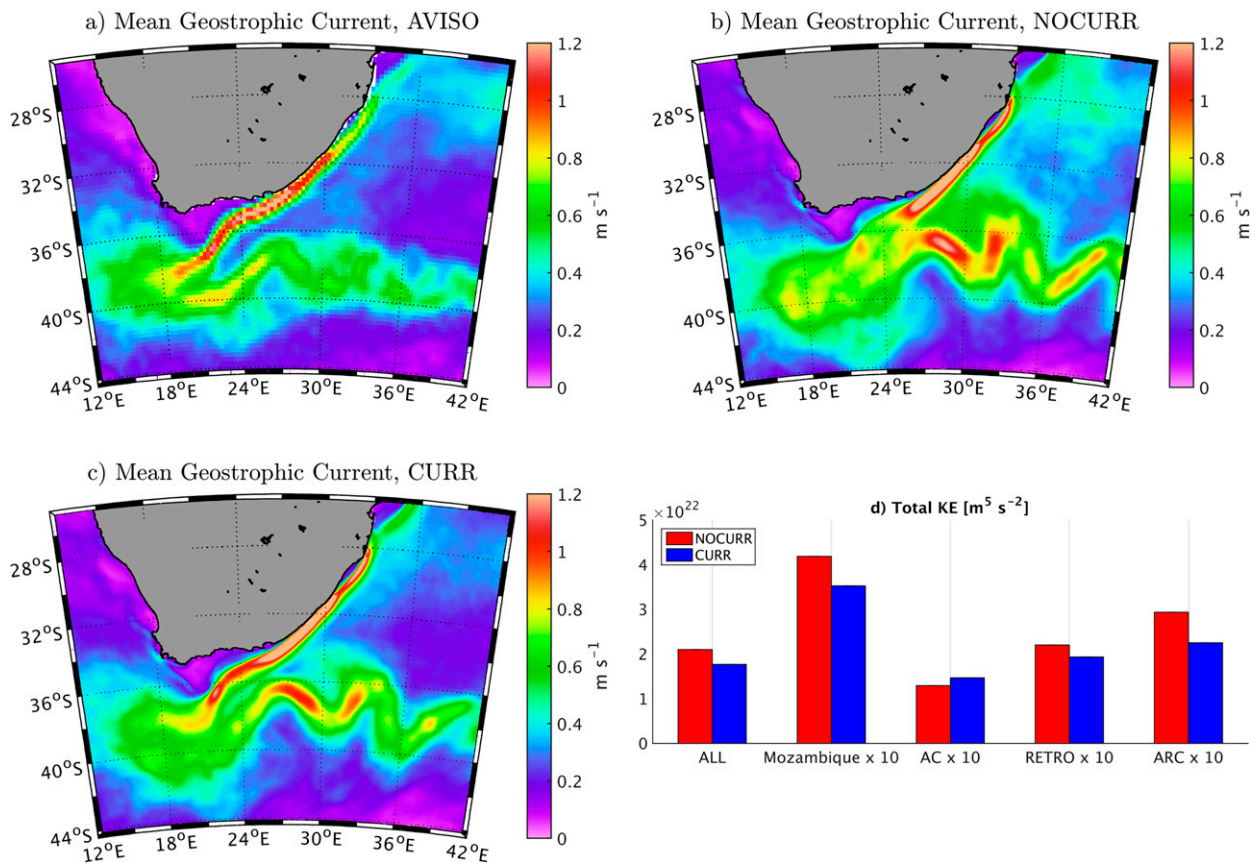


FIG. 4. Mean sea surface geostrophic currents from (a) AVISO, (b) NOCURR, and (c) CURR for the period 2000–04. (d) Total depth-integrated KE over the whole domain, the Mozambique Channel, and the Agulhas Basin region (black boxes; Fig. 1a). In (d) the Mozambique, AC, RETRO, and ARC values have been multiplied by a factor 10 to match the y scale. In CURR, the weakening of the mean wind work ($F_m K_{mg}$) induces a global slowdown of the circulation. However, because of a less present eastern retroflexion of the Agulhas Current, the Agulhas Current over the Agulhas Basin has a larger mean flow in CURR with respect to NOCURR. The Agulhas retroflexion is more realistic in CURR than in NOCURR.

the interactions between the AC and the Benguela Current. As pointed out by, for example, Penven (2000), in both simulations and AVISO, the currents are weak on the Agulhas Bank. As for the North Atlantic basin (Renault et al. 2016c), the reduction of $F_m K_{mg}$ globally slows down the mean circulation and hence reduces the KE by 16%, 15%, 13%, and 20% over the whole domain, the Mozambique Channel, the AC retroflexion, and the ARC, respectively (Fig. 4d). The slowdown of the circulation, and hence the weakening of the geostrophic surface currents, associated with the surface stress changes explains the reduction of $F_m K_{mg}$ from NOCURR to CURR. Finally, at 32°S, NOCURR and CURR simulate a southward transport of 81 and 78 Sv, respectively, which is consistent with Beal et al. (2015) and with the Biastoch et al. (2009) results for the 2000–04 period (Fig. 9 from Biastoch et al. 2009). As shown in Renault et al. (2016c), over a larger domain the current feedback may slow down the circulation over

the full Indian Gyre, which could further reduce the AC transport and KE.

b. Geostrophic eddy kinetic energy and mean pathway of energy from the ocean to the atmosphere

For the EKE analysis, five regions of interests are considered (Figs. 5a,d): the whole domain, the Mozambique Channel, the AC retroflexion, the ARC, and a box over an extended Benguela region. The surface geostrophic EKE is estimated using the daily geostrophic surface current perturbations from AVISO and from the experiments (Fig. 5). The EKE is larger over the Agulhas Basin south of South Africa and over the Mozambique Channel [in agreement with the literature, e.g., Ducet et al. (2000) and Penven et al. (2006)]. NOCURR overestimates the EKE with respect to AVISO over the whole domain by 75% and, in particular, by 59%, 47%, 77%, and 40% over the

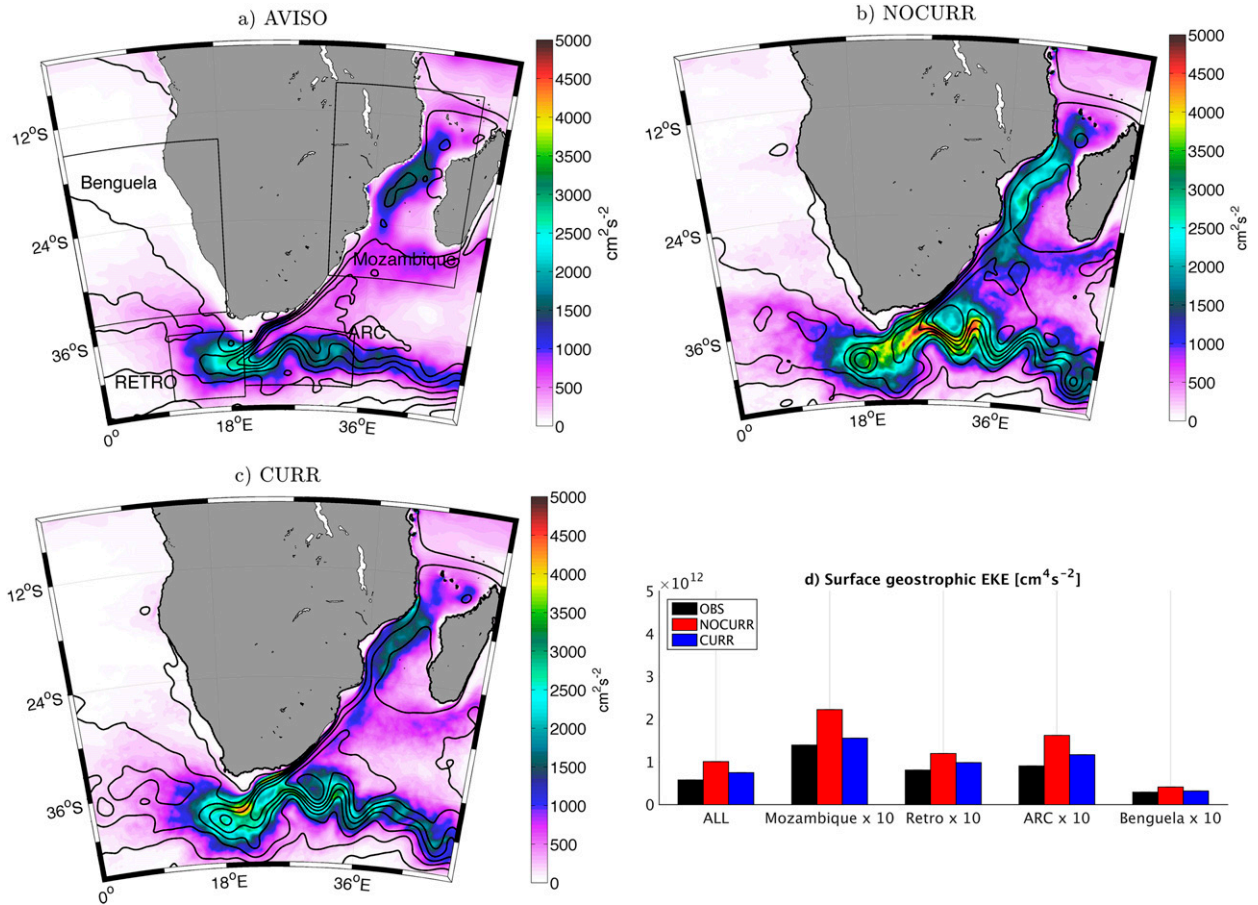


FIG. 5. Mean geostrophic EKE (color) for the period 2000–04 from (a) AVISO, (b) NOCURR, and (c) CURR. Contours show 20-cm delineations of mean sea surface height for this period. NOCURR is characterized by a too large EKE and by the presence of a standing eddy around the east of the Agulhas Basin that has a strong influence on the retroflection (see Fig. 9). (d) Mean EKE over the whole domain, the Mozambique Channel, the AC retroflection, the ARC, and the Benguela [black boxes in (a)]. In (d) the Mozambique, AC, RETRO, and ARC values have been multiplied by a factor 10 to match the y scale. The current feedback in CURR induces a drastic reduction of the EKE by 25% over the whole domain. It limits the presence of the standing eddies, improving the realism of the mean circulation and of the Agulhas Current retroflection.

Mozambique Channel, the AC retroflection, the ARC, and the Benguela, respectively. This could be partly explained by the smoothing used in AVISO. There are eddies in the real ocean that have scales smaller than can be resolved by the AVISO dataset (e.g., Chelton and Schlax 2003). However, a significant portion of the discrepancy is due to the lack of current feedback in NOCURR that, as shown in Figs. 6 and 7, induces a deflection of energy from the ocean to the atmosphere at eddy time scale. From NOCURR to CURR, the EKE is reduced by 25% over the whole domain and, in particular, by 30%, 17%, 28%, and 22% over the Mozambique Channel, the AC retroflection, the ARC, and the Benguela region, largely improving the realism of the simulation. The EKE in both NOCURR and CURR is larger than the EKE estimated by Loveday et al. (2014); this is likely due to a smoother topography in their

model and to their coarser spatial resolution [9.2 km over the Agulhas retroflection in Loveday et al. (2014) vs 4.8 km here].

Figure 6 depicts the relevant eddy-mean conversion terms estimated from NOCURR and CURR. Consistent with, for example, Halo et al. (2014), the barotropic conversion from mean to eddy $K_m K_e$ is the main driver of the EKE over the Mozambique Channel. It generates the Natal pulses that can induce upstream retroflections of the AC (e.g., Lutjeharms and Van Ballegooyen 1988a; Rouault and Penven 2011). The EKE over the Agulhas Basin region is partly driven by the Natal pulses advected from the Mozambique Channel (Biaستoch et al. 2009; Rouault and Penven 2011) but also driven locally by $K_m K_e$ (Fig. 6). Finally, for the Benguela, unlike the other eastern boundary upwelling systems, the mesoscale activity does not originate from the coast but

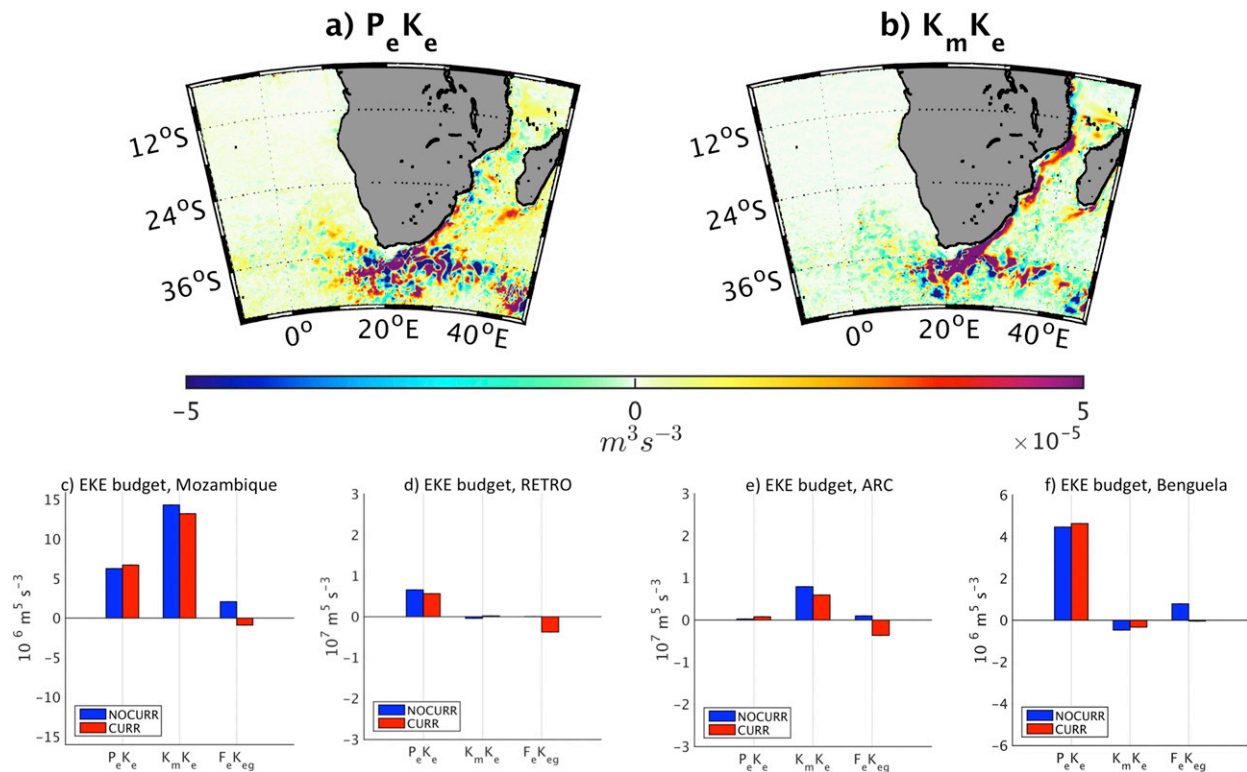


FIG. 6. (top) Depth-integrated EKE budget component ($\text{m}^3 \text{s}^{-3}$) from CURR. (a) The baroclinic conversion $P_e K_e$ and (b) the barotropic conversion $K_m K_e$. (bottom) Total $P_e K_e$, $K_m K_e$, and the eddy wind work $F_e K_{eg}$ integrated over (c) the Mozambique Channel, (d) the Agulhas retroflection (Retro), (e) the ARC, and (f) the Benguela (black boxes; Fig. 5a). $K_m K_e$ is the main energy source term. The reduction of the EKE from NOCURR to CURR in Fig. 5 is partly explained by the reduction of $K_m K_e$ but overall by the negative $F_e K_{eg}$.

from the shedding of rings and eddies at the AC retroflection (Matano and Beier 2003; Veitch et al. 2010).

Two pathways of energy can explain the EKE reduction from NOCURR to CURR. Figures 6c and 6d show the mean $P_e K_e$ and $K_m K_e$ integrated over the Mozambique Channel, the AC retroflection, the ARC, and the Benguela (black boxes in Fig. 5a). First, there is a reduction of the available mean energy over the whole domain (due to the reduction of $F_m K_{mg}$). This causes a reduction of the barotropic conversion from mean kinetic energy to EKE ($K_m K_e$) over the whole domain (by 15%) but also specifically over the Mozambique Channel and the ARC (by 8% and 17%, respectively), whereas $P_e K_e$ is barely impacted (up to 5% over the Mozambique Channel). The EKE reduction of the Agulhas Basin region is thus partly explained by the local reduction of $K_m K_e$ and partly by a reduction of the Natal pulses generation in the Natal Bight. The second pathway of energy is a mechanical dampening (e.g., Dewar and Flierl 1987; Duhaut and Straub 2006; Dawe and Thompson 2006; Eden and Dietze 2009), that is, a deflection of energy from the oceanic geostrophic currents (eddies) to the

atmosphere, which acts as an eddy killer (Renault et al. 2016d). Over an oceanic eddy, when taking into account the surface current into the estimation of the surface stress, there is a reduction of the positive $F_e K_{eg}$ and an increase of the negative $F_e K_{eg}$, leading to a net negative $F_e K_{eg}$. In Fig. 7, $F_e K_{eg}$ is estimated from the experiments and by using the geostrophic currents from AVISO and the surface stress from a QuikSCAT product (Bentamy et al. 2013). Along the coast, the wind perturbations induce an offshore Ekman surface current and an oceanic coastal jet (e.g., Renault et al. 2012) that partially flows in the same direction as the wind, inducing a positive $F_e K_{eg}$ (Renault et al. 2016d). In agreement with the literature (e.g., Renault et al. 2016c; Scott and Xu 2009; Xu et al. 2016), the observations also reveal a pathway of energy from the ocean to the atmosphere over all the domain and in particular over the Agulhas Basin region. This large-scale pathway of energy from the ocean to the atmosphere is induced by the current feedback. CURR has slightly larger values of $F_e K_{eg}$ with respect to the observation estimate (by 5%); this may be certainly explained by model biases (e.g., too large an EKE would deflect too

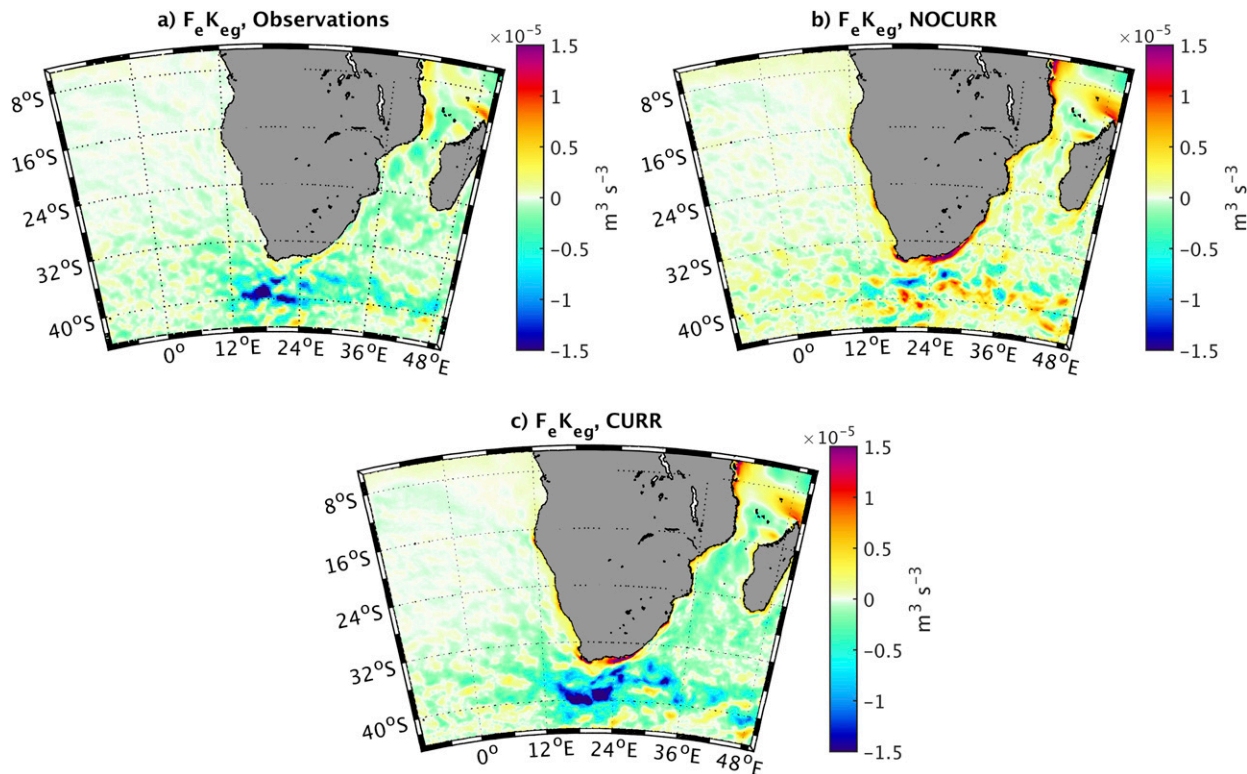


FIG. 7. Mean geostrophic eddy wind work $F_e K_{eg}$ from (a) the observations, (b) NOCURR, and (c) CURR for the period 2000–04. The observations and CURR are characterized by the presence of a pathway of energy from the ocean to the atmosphere all over the Agulhas Current, which is not present in NOCURR. The negative $F_e K_{eg}$ is partly responsible for the dampening of the EKE in Fig. 5.

large amount of energy from the ocean to the atmosphere) but also may be explained by the smoothing used in AVISO (e.g., Chelton and Schlax 2003). NOCURR does not reproduce the negative $F_e K_{eg}$ because it ignores the currents influence on the surface stress. The terms $F_e K_{eg}$ and $K_m K_e$ are the main drivers of the EKE reduction from NOCURR to CURR over the Mozambique Channel and over the Agulhas Basin (both AC retroflection and ARC), with $F_e K_{eg}$ having the main contribution. Finally, for the Benguela, because most of the mesoscale activity originates from the shedding of rings and eddies in the AC retroflection (Matano and Beier 2003; Veitch et al. 2010), the reduction of the EKE over the Agulhas Basin and the eddy killing (negative $F_e K_{eg}$) explain the EKE reduction from NOCURR to CURR. The negative $F_e K_{eg}$ is by definition linked to the current feedback [Eq. (5)] because the surface stress is estimated using the surface current [Eqs. (2) and (3)]. For instance, the monthly time series of EKE and $F_e K_{eg}$ averaged over the ARC box have a temporal correlation of 0.7 ($\sigma > 95\%$, not shown). Here, again, the seasonal cycle of the wind that can induce a change locally in wind direction is not relevant. The negativeness of $F_e K_{eg}$ when using the

current feedback does not depend on the wind direction (see Fig. 5 from Renault et al. 2016d).

c. Ageostrophic response

The current feedback effect on the geostrophic wind work and its consequences on the oceanic circulation are the main focus of this study. However, the current feedback can also influence the ageostrophic motions. First, the reduction of the mean surface stress induces a weakening of the Ekman current by roughly 8% (not shown). More interesting, the current feedback to the atmosphere may have an effect on the submesoscale motions. A reduction of the mesoscale activity weakens the frontogenesis activity and thus the submesoscale motions. Figure 8 depicts the 2D KE spectra and 2D ageostrophic KE spectra as a function of wavelength (km) from NOCURR and CURR over the Mozambique Channel, the Agulhas Basin, and the Benguela. We defined the energy spectra change $C_{\text{spectra}} = [(CURR - NOCURR)/CURR] \times 100$ as the relative change between NOCURR and CURR. A negative C_{spectra} indicates a reduction of the energy from NOCURR to CURR. The ageostrophic submesoscale energy is reduced by 20% over the Mozambique and the Agulhas Basin; the effect over the Benguela region is

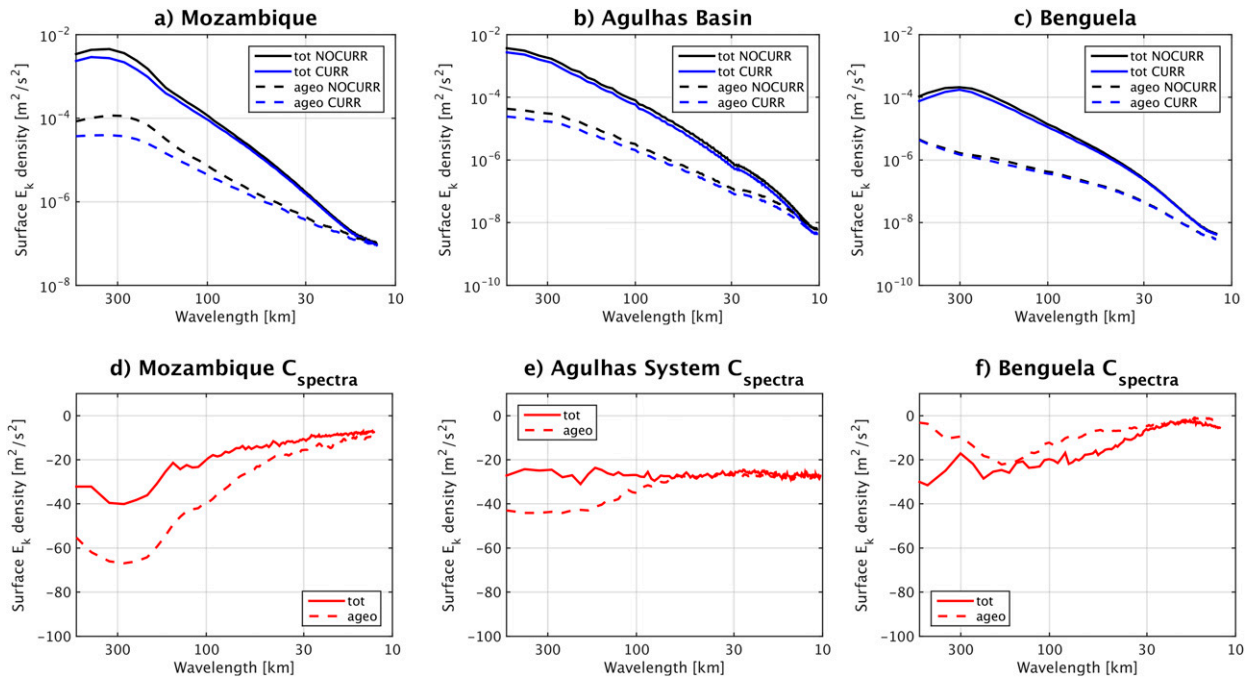


FIG. 8. (top) The 2D total (solid) and ageostrophic (dashed) surface KE spectra as a function of the wavelength (km) for NOCURR (black) and CURR (blue) and (bottom) their relative difference C_{spectra} . (a),(d) Over the Mozambique Channel, (b),(e) the Agulhas Basin, and (c),(f) the Benguela. By reducing the mesoscale activity, the current feedback weakens the frontogenesis and diminishes the submesoscale activity. These results should be confirmed using higher spatial resolution configurations.

weaker because of a less pronounced reduction of the EKE over that region. The model used here is only sub-mesoscale permitting ($dx = 5$ km), this indirect impact should be further assessed by using a nesting procedure approach allowing a very high spatial resolution over the Agulhas Basin, as in, for example, Capet et al. (2008b) for the U.S. West Coast.

4. Mean Agulhas retroflection and leakage

a. Agulhas retroflection

The lack of current feedback acts on the circulation through two direct effects: a reduction of the $F_m K_{mg}$ with a slowdown of the circulation and a dampening of the mesoscale activity. Those changes have an impact on the AC retroflection. Figure 5 depicts the mean SSH from AVISO and from the experiments. NOCURR is characterized by the presence of two too persistent standing eddies nearby Port Elizabeth (around 36°S , 32°E) and over the AC retroflection. The eastern standing eddy is induced by the Natal pulses that propagate from the Natal Bight and eventually merge with the AC near Port Elizabeth (e.g., Rouault and Penven 2011) but also from eddies from the ARC, which detach and propagate westward (McWilliams 1985) toward Port Elizabeth

where they can die, merge, and/or recirculate. This process is thought to induce upstream retroflection of the AC (Lutjeharms and Van Ballegooyen 1988a). The western standing eddy induces a southern location of the AC retroflection with respect to AVISO. In CURR, the dampening of the EKE by negative $F_e K_e$ (eddy killing) and also by the reduction of $K_m K_e$ (that reduces the generation of the Natal pulses) weakens the persistence of the two standing eddies, improving the realism of the AC mean path and its retroflection with respect to AVISO. In particular, the retroflection is shifted toward the north, improving its realism (see Fig. 4).

As in Backeberg et al. (2012) and Loveday et al. (2014), the retroflection extent is derived for the period 2000–04 via a sea surface height contour from AVISO and from the simulations (section 2e and Fig. 9d). Retroflection position distributions are then spatially binned into 0.5° longitudinal boxes [bins are determined using a Freedman–Diaconis rule (Freedman and Diaconis 1981)], producing a zonal probability density function for AVISO and for each experiment (Figs. 9a,b,c). The peaks' significance is assessed using a bootstrap method; the probability density function of the retroflection position is computed 100 000 times using random samples from the distribution. The error bars are defined as plus or minus the standard deviation of the obtained

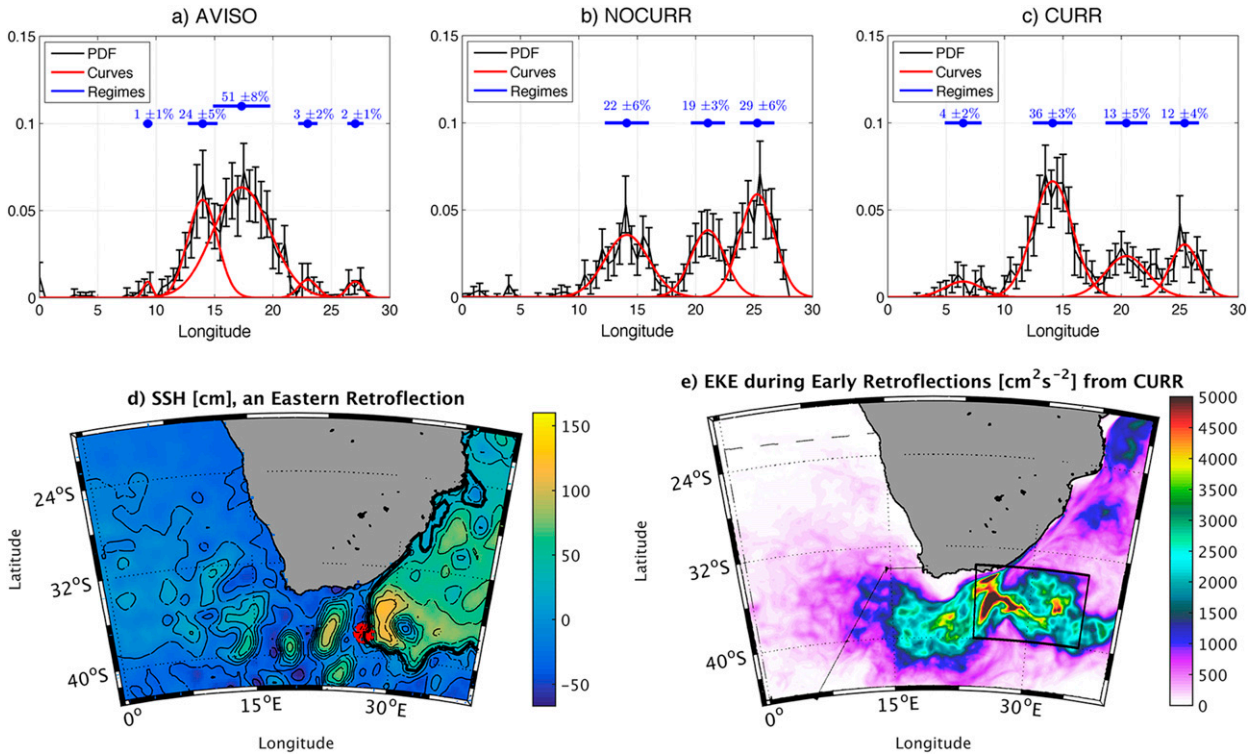


FIG. 9. (a) Zonal probability density function (PDF) of the retroreflection location for the period 2000–04 from (a) AVISO, (b) NOCURR, and (c) CURR. The black lines represent the PDF values and their standard deviations obtained using a bootstrap method (see text). The red lines represent the Gaussian fits applied on the significant PDF peaks. The blue circles highlight the center of each regime (i.e., the peaks of the PDF), and the blue lines represent the spatial extension of each regime as estimated from the standard deviation of the Gaussian fits. The percent of occurrences of each regime is indicated in blue (see text for more details). The current feedback to the atmosphere improves the representation of the Agulhas Current retroreflection. In particular, by weakening the mesoscale activity, it strongly reduces the importance of the eastern retroreflections, shifting the distribution of the retroreflection location. (d) Illustration of an Agulhas Current eastern retroreflection from AVISO as estimated by the detection method (section 2e). The colors represent the SSH from AVISO; the thick black contour represents the detected Agulhas current and the red dot its retroreflection longitude and latitude. (e) Mean eddy kinetic energy during the eastern retroreflections. The black box is used in Fig. 10. The solid line represents the shipping line (Good Hope line) section, whereas the dotted lines represent the control sections used to estimate the Agulhas Current leakage using Lagrangian particles.

bins values. To determine the regimes of variability of the AC retroreflection, Gaussian fits are then applied on the significant peaks of the probability density function. The spatial extensions of the regimes are derived from the standard deviation of the Gaussian fits plus or minus their 95% significant bounds.

The AVISO zonal probability density function (Fig. 9a) is largely characterized by the presence of the five regimes of variability. The two first dominant regimes are characterized by a central AC retroreflection between 15.2° and 20°E (mean at 17.3°E) in 51% of the occurrences for the first regime and by a western retroreflection between 12.5° and 15.3°E (mean at 14°E) in 24% of the occurrences for the second regime. The probability density function highlights two other kinds of retroreflections: another western retroreflection (mean at 9.2°E) in 1% of the occurrences and an eastern retroreflection (or upstream; Fig. 9d) defined

by two regimes of variability around 23°E and 27°W, representing 3% and 2% of the occurrences, respectively.

Numerical models have persistent issues realistically representing the AC retroreflection and its variability (e.g., Loveday et al. 2014). From NOCURR to CURR, there is a westward shift of the mean AC retroreflection (Fig. 4). NOCURR simulates the mean position of the AC retroreflection around 19.5°E with a too large zonal variability of its reflection with respect to the observations (Fig. 9). Part of the discrepancies in NOCURR comes from a poor representation of the regime of AC retroreflection variability; the dominant regimes are the two eastern retroreflections (29% and 19%). The central retroreflection does not have a peak in the probability density function estimated from NOCURR. It is included in an eastern retroreflection mode, representing 22% of the occurrences. The eastern retroreflection is believed to be induced by the

Natal pulses, which merge near Port Elizabeth and cause a shortcut of the AC (Biaostoch et al. 2008c; Rouault and Penven 2011). It could also be due to eddies from the ARC, which detach and propagate westward (McWilliams 1985) toward Port Elizabeth where they can die, merge, and/or recirculate. The too strong mesoscale activity in NOCURRE reinforces the eastern category (i.e., the upstream AC retroflection).

In CURR, the weakening of the mesoscale activity improves the representation of the AC retroflection, despite some persistent biases. The mean AC position is very close to the observations, around 15.3°E, but, as in NOCURRE, it has a too large variability. The current feedback in CURR dampens the EKE and, in particular, the Natal pulses and their influence on the EKE over the Agulhas Basin. This diminishes the importance of the eastern retroflection regimes, allowing a shift toward the west of the retroflection distribution. Indeed, in CURR, the main regime of variability is the eastern retroflection that, as in NOCURRE, also includes the central retroflection detected from the observations (between 13° and 16°E). The other western retroflection is centered at 6.5°E and is slightly overrepresented (4%). The remaining overrepresentation of the eastern retroflection is likely due to an overestimation of the EKE in CURR that may be the consequence of the biases in $F_m K_{mg}$ and too large a $K_m K_e$ (Figs. 1, 6). Figure 9e depicts the mean EKE averaged over the eastern regime mode periods. The very large anomalies of EKE near Port Elizabeth (more than twice the long-term mean values) likely induce a shortcut of the AC and thus an eastern AC retroflection. This relationship between EKE and AC is in good agreement with Backeberg et al. (2012) and Beal and Elipot (2016). Finally, to discard an eventual effect of the atmospheric forcing in our simulation (WRF) on the representation of the third category (eastern retroflection), an additional uncoupled simulation has been carried out using climatological forcing (e.g., QuikSCAT stress), as in, for example, Capet et al. (2008a), with the same spatial resolution as NOCURRE and CURR. That simulation has similar characteristics to NOCURRE in terms of EKE and AC retroflection and, in particular, has an overestimation of the standing eddies.

b. Mean Agulhas Current leakage

The AC leakage is difficult to estimate. Observations and numerical models present a wide range of estimates varying from 2 to 15 Sv (de Ruijter et al. 1999a; Richardson 2007; Rouault et al. 2009; van Sebille et al. 2010; Chen et al. 2016). Van Sebille et al. (2010) apply a method developed by Rouault et al. (2009) to estimate the AC leakage based on an estimation of the Eulerian

transport of discriminate temperature ($\Theta > 14.6^\circ$) and salinity ($\Sigma > 35.33$). The Eulerian flux $F_{\Theta\Sigma}$ as a function of threshold temperature and threshold salinity is

$$F_{\Theta\Sigma} = \int_{\theta=\Theta}^{\infty} \int_{\sigma=\Sigma}^{\infty} V(\theta, \sigma) d\sigma d\theta, \quad (8)$$

where $V(\theta, \sigma)d\sigma d\theta$ is the flux through all grid cells with temperature θ and salinity σ . In NOCURRE and CURR, through the Good Hope line, $F_{\Theta\Sigma}$ is 5.0 and 6.1 Sv, respectively, which is comparable to the estimates from van Sebille et al. (2010). The magnitude of the AC leakage is underestimated by $F_{\Theta\Sigma}$; however, van Sebille et al. (2010) demonstrate the existence of a linear relationship between the total magnitude of Agulhas leakage and $F_{\Theta\Sigma}$:

$$E_{AL} = 2F_{\Theta\Sigma} + 1.9 \text{ Sv}. \quad (9)$$

Using Eq. (9), the total AC leakage from NOCURRE and CURR is 11.9 and 14.1 Sv, respectively, which are both weaker than the van Sebille et al. (2010) estimates but similar to the recent estimates from Chen et al. (2016). This may be due to the overrepresentation of the upstream retroflection. However, both NOCURRE and CURR estimated leakages are within the wide range of previous estimates (de Ruijter et al. 1999a; Richardson 2007; van Sebille et al. 2010). The changes from NOCURRE to CURR (although the current feedback to the atmosphere weakens the EKE and slows down the circulation) lead to an increase of the Agulhas leakage. This counterintuitive result is consistent with the reduction of the AC eastern retroflection regimes from NOCURRE to CURR. The AC retroflection is more often around 15°E, allowing a larger leakage into the Atlantic Ocean; this is consistent with the van Sebille et al. (2009) finding.

As discussed in, for example, Beal et al. (2011), there are still uncertainties on the origin of the leakage variations. Here, as shown in Fig. 9e, the eastern retroflections are linked to the presence of large EKE values near Port Elizabeth that short-cut the AC. Therefore, there is a possible link between the EKE near Port Elizabeth and the AC leakage. Using CURR, the time series of EKE and $F_e K_{eg}$ have been computed over the region, where the EKE is large during the eastern retroflection (black box in Fig. 9e). The resulting time series and the leakage are then low-pass filtered ($f_c = 180 \text{ days}^{-1}$). Lag correlations between the EKE and the leakage are finally computed (Fig. 10). First, not surprising, a large significant ($\sigma > 95\%$) correlation of 0.93 is found between the EKE temporal variations and $F_e K_{eg}$. A large EKE induces a large transfer of energy from the ocean to the atmosphere (negative $F_e K_{eg}$). More interesting, a large significant ($\sigma > 95\%$) correlation of 0.46 is found

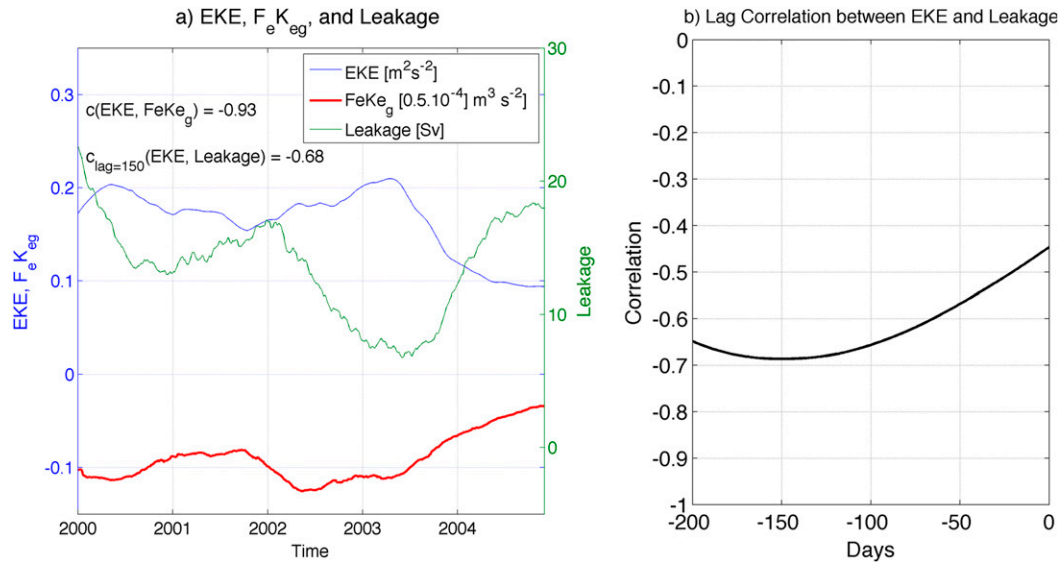


FIG. 10. Relationship between the EKE, the eddy wind work $F_e K_{eg}$, and the leakage from CURR. The EKE and $F_e K_{eg}$ have been spatially average over the box indicated in Fig. 9c. (a) The resulting time series and the leakage time series have been low-pass filtered ($f_c = 180 \text{ days}^{-1}$). (b) The lag correlation between EKE and leakage. A large EKE near Port Elizabeth induces a large deflection of energy from the ocean to the atmosphere but also a shortcut of the Agulhas Current and then a weakening of the Agulhas Current leakage.

between the EKE and the leakage. Using a lag of 150 days between the EKE and the leakage, the correlation increases to 0.68 ($\sigma > 95\%$). The EKE grows in that region likely due to a barotropic generation of eddies and the merging of Natal pulses and eddies detaching from the ARC and propagating westward. To some extent the EKE activity becomes large enough to short-cut the AC, weakening the AC leakage. A similar relationship is found using NOCURR (not shown). From NOCURR to CURR, the weakening of the EKE driven by the negative $F_e K_{eg}$ leads to a large reduction of the EKE, and then to an increase of the AC leakage. This is consistent with van Leeuwen et al. (2000) and also with van Sebille et al. (2009) that show a more frequent westward retroflection leads to more leakage but not with Biastoch et al. (2008c), who suggest Natal pulses and the induced upstream retroflection do not have an influence on the AC leakage. Our results are also partially in disagreement with Rouault et al. (2009), who show (using a 0.25° oceanic model) an increase in the leakage is associated with an increase in Agulhas Current transport near Port Elizabeth. From NOCURR to CURR, the AC is weakened at 32°S but is increased downstream of Port Elizabeth.

Finally, to confirm the leakage estimates and the alteration of the Agulhas rings corridor by the current feedback, the trajectories of numerical Lagrangian floats are integrated using the ARIANE package (Blanke et al. 1999). Similar to, for example, Biastoch

et al. (2008b) and van Sebille et al. (2010), particles are seeded every day in a 300-km zonal section of the Agulhas Current core at 32°S (up to 1500-m depth, about 3×10^6 particles in total). Then, the particles are advected using the daily mean velocity fields over a time span of 4.5 years (2000–04) in NOCURR and CURR and intercepted along the section depicted in Fig. 9e. Two sections are considered in the South Atlantic Ocean: one along 0° up from 45° to 25°S , and one along 25°S from 0° to the coast. An average leakage is then evaluated by ARIANE by counting the particles that flow through the control sections in the Atlantic Ocean. In the simulation without current feedback (i.e., NOCURR), about 10.6 Sv reaches the northern/western sections in the Atlantic, whereas 12.9 Sv reaches them in CURR. Consistent with our previous results, the current feedback in CURR allows a larger leakage of the AC of about 2.3 Sv (21%). In CURR, the western offshore leakage is larger by 2.0 Sv (from 8.5 to 10.5 Sv) and by 0.3 Sv through the northern section (from 2.1 to 2.4 Sv). Both estimates are within the wide range of leakage estimates (from 2 to 15 Sv) from the observations and numerical models (de Ruijter et al. 1999a; Gordon 2003; Richardson 2007; van Sebille et al. 2009; Biastoch et al. 2008c,b,a; Putrasahan et al. 2015; Chen et al. 2016). Our previous estimates, based on the method developed by Rouault et al. (2009), predict a larger leakage in both simulations (11.9 and 14.1 Sv in NOCURR and CURR, respectively); however, the differences are within the

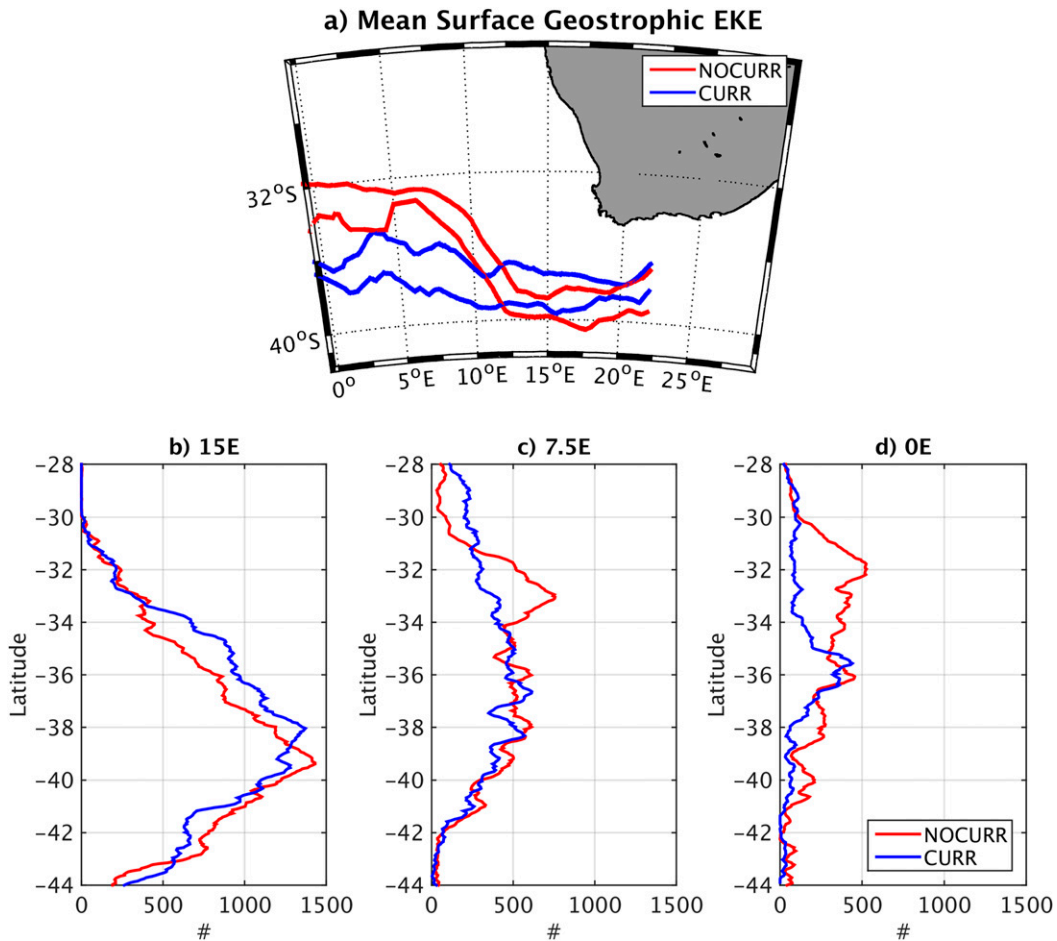


FIG. 11. (a) Mean Agulhas rings corridor identified using the mean surface geostrophic EKE from NOCURR (red) and CURR (blue) for the period 2000–04. The contour lines corresponds to the maximal mean EKE value along each longitude and to 90% of the maximal EKE value along each longitude; the contour lines are smoothed over a distance of 150 km. (b) Meridional distribution of the surface geostrophic EKE (Fig. 5) along three sections at 15°E, 7.5°E, and 0° from NOCURR (red) and CURR (blue). For each daily snapshot over the period 2000–04, the EKE distribution is estimated using bin sizes of $0.05 \text{ m}^2 \text{ s}^{-2}$. The current feedback alters the Agulhas rings corridor.

confidence band of 11.6 Sv for that method (van Sebille et al. 2010).

c. Mean pathway of the Agulhas Current leakage

By modulating the circulation over the Agulhas Basin region, the current feedback to the atmosphere modulates the AC retroflection position and the AC leakage itself. As shown by Renault et al. (2016d), the current feedback reduces the eddy life and rotational speed and limits their offshore propagation. It may therefore significantly alter the propagation of the Agulhas rings and change their mean corridor of propagation, spreading in a different way the saltier and warmer water of the Indian Ocean into the South Atlantic Ocean. The Agulhas rings corridor is first evaluated by determining the envelope of the mean geostrophic EKE larger than 90% of its maximal latitudinal value from each experiment (Fig. 11a).

The 90% EKE envelope is then zonally smoothed over a distance of 150 km. The surface geostrophic EKE used here is mainly due to the Agulhas rings; the Agulhas cyclones are weaker, propagate southwestward counter to the South Atlantic Current, and do not translate as far as the rings (Richardson 2007). In both simulations, the Agulhas rings go north as they move west. However, the current feedback clearly alters the way they propagate and therefore the Agulhas rings corridor. There are two main impacts. First, in CURR, the shedding of the eddies is shifted about 1.1° toward the north with respect to NOCURR, and its orientation is less southward. This is consistent with Fig. 5, which depicts a mean retroflection located more to the south in NOCURR. Second, in CURR, the Agulhas rings are dampened by the current feedback and then go less far north than in NOCURR; at 15° to 5°E, the 90% EKE is centered around 39° and 33°S

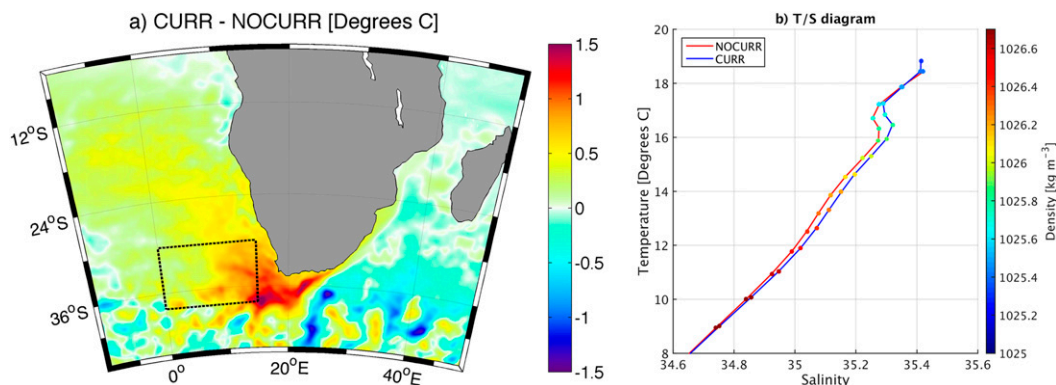


FIG. 12. (a) Mean SST difference between CURR and NOCURR. (b) Temperature–salinity diagram from NOCURR (red) and CURR (blue) over the black box represented in (a) and averaged over bins of constant potential density of 0.1 kg m^{-3} . The dashed black lines depict the region used to evaluate the temperature–salinity diagram. The colors represent the potential density. In CURR, because of a larger leakage, there is saltier and warmer water between 800- and 200-m depth and warmer sea surface temperature.

in NOCURR. In CURR, it is centered around 38° and 36°S . Farther west than 5°W , the mean EKE in CURR is too weak to draw any conclusion.

To confirm the alteration of the Agulhas rings corridor, the meridional distribution of the surface geostrophic EKE is evaluated along three sections at 15°E , 7.5°E , and 0° (Fig. 11b). For each daily snapshot over the period 2000–04, the EKE distribution is estimated using bin sizes of $0.05 \text{ m}^2 \text{ s}^{-2}$. In CURR, at 15°E , consistent with the other results, the shedding of the eddies is situated at 38° versus 39.4°S in NOCURR. The Agulhas rings in CURR go less far north than the ones in NOCURR. In NOCURR, the largest EKE regions are situated around 39.4° , 33° , and 32°S , along the sections at 15°E , 7.5°E , and 0° , whereas in CURR, the largest EKE distribution is around 38°S at 15°E , and then it is situated at 36.5° and 35.4°S along the section 7.5°E and 0° . This is confirmed by the particles analysis of the previous section. The particles intercepted at the western section (i.e., the section along 0°) are centered around 32.2° and 34.8°S in NOCURR and CURR, respectively. Similar results are found using the salinity at 1000-m depth as a tracer.

d. Water masses changes

The changes of AC leakage and the Agulhas rings corridor have an impact on the spread of the warmer and saltier water masses from the Indian Ocean into the South Atlantic Ocean. Figure 12a depicts the mean SST difference between NOCURR and CURR. CURR has a warmer SST over the Agulhas Basin region (up to 1.5°C) and over the Benguela upwelling system (0.8°C). As a result, the mean SST gradients over the Agulhas retro-reflection are also larger in CURR with respect to NOCURR. The net heat flux over the Agulhas Basin is more negative in CURR than in NOCURR (by 10%,

mostly driven by the turbulent heat fluxes), inducing a larger heat transfer from the ocean to the atmosphere. It is not significantly changed over the Benguela region. The warming of the Benguela and of the Agulhas Basin is actually explained by a larger transport of warm water from the Indian Ocean to the Atlantic Ocean in CURR with respect to NOCURR. First, along the Agulhas Basin, the AC is more intense, and rings carry warmer surface water from the Indian Ocean. That explains the warmer SST and the larger negative turbulent fluxes over the Agulhas Basin. Second, the larger leakage and the more intense Good Hope jet bring warmer surface water into the Benguela upwelling system. In Fig. 12b, a binned temperature–salinity diagram exposes the mean hydrological characteristics of the water masses of the South Atlantic from the simulations (see box in Fig. 12a). The temperature and salinity values are computed by averaging the temperature and salinity over bins of potential density of 0.1 kg m^{-3} . Because the mean water masses are not significantly changed below 1000-m depth, only the water masses with a depth shallower than 1000 m are shown. In CURR, the stronger leakage provides warmer and saltier water at depth between 800 and 200 m and, consistent with Fig. 12a, warmer water at the surface (by 0.8°C). From NOCURR to CURR, the changes in temperature at depth (up to 0.5°C at 500-m depth around the Good Hope line) are due to a larger temperature flux across the Good Hope line from NOCURR and CURR that increases from 0.4 to 0.48 PW. This is consistent with Rouault et al. (2009), who estimate the increase in the past two decades in Agulhas Current transport induces an interocean heat anomaly exchange increase of about $0.2 \text{ PW decade}^{-1}$, leading to a warming of the temperature up to $1.5^\circ\text{C decade}^{-1}$ at depth. The current feedback to the atmosphere has, therefore, two main impacts on

the Benguela. It reduces the mesoscale activity and alters its water mass properties, which could partly explain the SST biases reported by, for example, Veitch et al. (2010).

5. Atmospheric response

When coupling the atmosphere to the oceanic currents, the reduction in air–sea velocity difference reduces the stress acting on the wind and allows it to accelerate. In that sense, the oceanic surface currents partially drive the atmosphere, which in turn reenergizes the ocean (Renault et al. 2016d). As discussed in section 3c, the effect of the current feedback on the mean wind is clearly highlighted in Fig. 3. Over the Agulhas Current, a reduction of the surface stress induced an increase of the surface wind and vice versa. Renault et al. (2016d) demonstrate the existence of a linear relationship between the surface currents and the surface wind. They define the current–wind coupling coefficient s_w from the slope of that linear relationship. For the U.S. West Coast, Renault et al. (2016d) found a $s_w = 0.23$. Here, s_w is estimated at each grid point using the fully coupled experiment (CURR) over the period 2000–04; only the s_w with a $\sigma > 0.95$ using an F test is used. As in Renault et al. (2016d), the coastal band (150 km wide) is not taken into account because of the strong influence of the orography and coastline meandering on the wind that can hide the influence of the currents (Renault et al. 2016b). Figure 13a depicts the s_w spatial distribution smoothed over 100 km. It shows s_w is not constant and varies from 0.1 to 0.5 (nondimensional). Figure 13b depicts the structure of the coupling coefficient s_w over the Agulhas Return Current (similar behavior is found over other regions). There is a sharp vertical decay of the influence of the current on the wind; the current feedback mainly acts on the surface wind, but, consistent with Renault et al. (2016d), its effect can be felt up to 350 m. However, it remains weak with respect to the wind velocities (e.g., at 350 m, a s_w of 0.05 induces a wind response of 5 cm s^{-1} , which is weak compared to wind velocities of 15 m s^{-1}). The value of s_w depends on the current’s magnitude and on the background wind (Renault et al. 2016d; Gaube et al. 2015). It also depends on the marine boundary layer height. To highlight it, a binned scatterplot of the mean marine boundary layer height and s_w is estimated over the whole domain using bins of 50 m for the marine boundary layer height (Fig. 13c). It shows a clear linear relationship ($\sigma > 0.95$ using an F test) between the marine boundary layer height and s_w : a deeper Marine boundary layer induces a weaker s_w . This is consistent with Fig. 10 from Renault et al. (2016d), which shows the energy deflected from the ocean to the atmosphere by the current feedback that is distributed over the entire marine boundary layer.

From an atmospheric point of view, the current feedback-induced changes remain weak with respect to the wind velocities. However, the atmosphere can be influenced by indirect effects of the current feedback. As discussed in the previous section, from NOCURR to CURR, the SST over the AC retroflection and the southern Benguela warms up to 1.5° . This warms up the atmosphere and alters the mean precipitation from NOCURR to CURR. The change in mean precipitation over the period 2000–04 is defined as $C_{\text{rain}} = [(\text{rain}_{\text{CURR}} - \text{rain}_{\text{NOCURR}}) / \text{rain}_{\text{NOCURR}}] \times 100$. A positive C_{rain} indicates an increase of the precipitation from NOCURR to CURR. Only significant C_{rain} ($\sigma > 0.95$ using the Student’s t test) is shown in Fig. 14. Over the AC retroflection and the southern Benguela, from NOCURR to CURR the current feedback increases the precipitation rate by 50% (from 1.5 to 2.2 mm day^{-1} ; see Fig. 14). This may be caused by the warmer SST and associated larger SST gradients over the Agulhas retroflection in CURR. Further investigation is needed to clarify the impact of air–sea interactions on the precipitation (similar as, e.g., Kilpatrick et al. 2016). The other regions of the domain are not significantly impacted by the current feedback. The mean precipitation rate is fairly reproduced by the atmospheric model in both CURR and NOCURR (Fig. 14c). Over the ocean, the main spatial gradients are well reproduced with very weak precipitation over the southern Benguela region ($< 1 \text{ mm day}^{-1}$) and larger precipitation over the western part of the Agulhas Current system and, in particular, over the Agulhas Current, near Port Elizabeth ($> 3 \text{ mm day}^{-1}$). Over the land, the agreement between the satellite observations and the model is remarkable. Such a good agreement is confirmed by the high-resolution observations dataset from, for example, Harris et al. (2014) and Lynch (2004). For instance, the precipitation caused by convective cells over the Highveld Plateau is well reproduced (confirming the realism of the scheme used in the atmospheric model) as well as the arid region of the Northern Province and the local minimum of the Klein Karoo and northeast of Cederberg regions. Other variables such as mean cloud cover or mean marine boundary layer height are only marginally impacted by the SST changes from CURR to NOCURR (less than 5%, not shown). Note both simulations represent the SST feedback and therefore have SST large-scale and mesoscale feedbacks to the atmosphere.

6. Discussion and conclusions

Using oceanic and atmospheric coupled simulations, we assess how the current feedback to the atmosphere

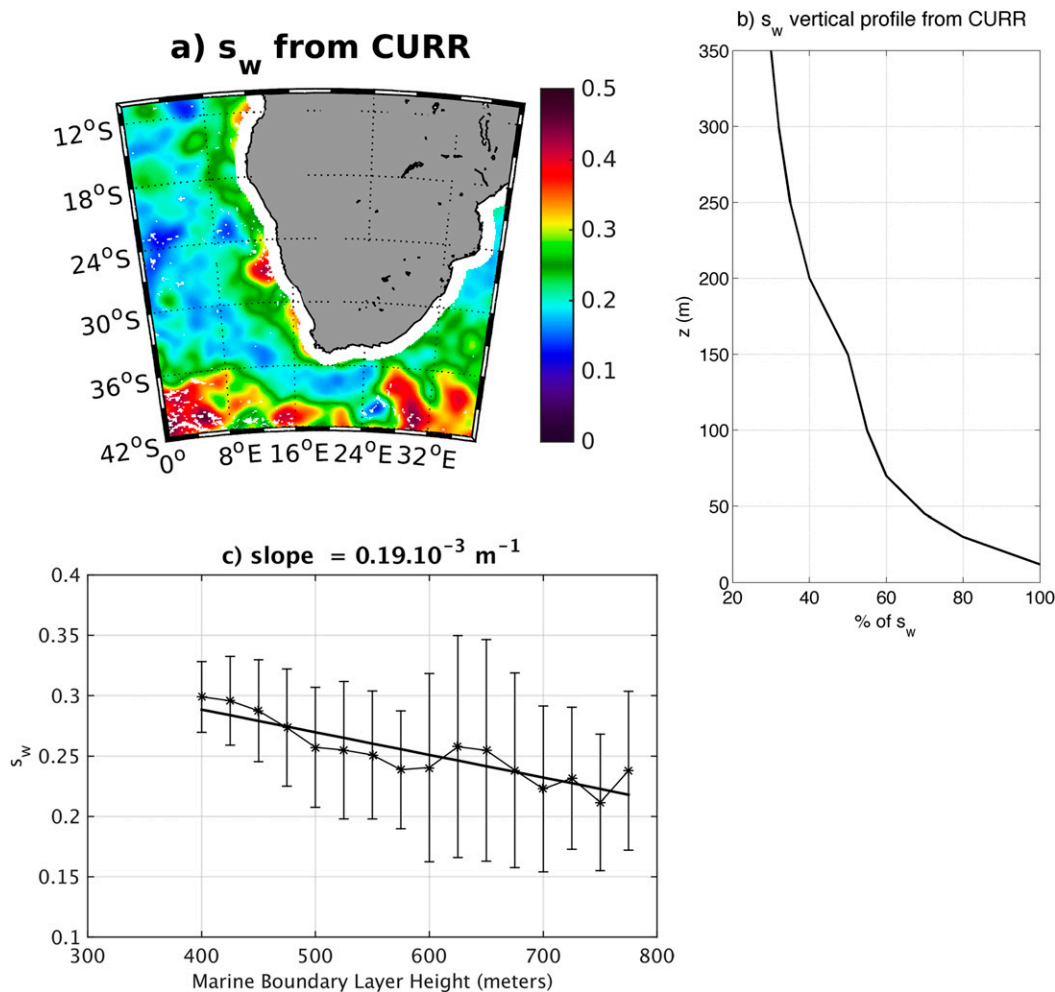


FIG. 13. (a) Current–wind coupling coefficient s_w estimated as in Renault et al. (2016d) at each grid point and smoothed over 100 km. (b) Vertical attenuation of s_w with respect to the surface s_w over the Agulhas Return Current box (similar results are found for other regions). (c) Binned scatterplot of the mean marine boundary layer height and s_w over the whole domain. The bars indicate plus and minus one std dev about the average drawn by stars. The linear regression is indicated by a black line, and the slope is indicated in the title ($0.19 \times 10^{-3} \text{ m}^{-1}$). The coefficient s_w is characterized by a complex spatial pattern that depends on the marine boundary layer height. The deeper the marine boundary layer is, the weaker s_w is. The current feedback to the atmosphere mainly acts on the surface wind.

modulates the transfer of energy between the atmosphere and the ocean (wind work) and how it alters the Agulhas Current (AC) retroflection and leakage. Our results on the modulation of the wind work by the current feedback can be compared to the findings of Renault et al. (2016d,c). Here, the current feedback attenuates the mean transfer of energy from the atmosphere to the ocean (mean wind work) by 12%. This is less than the weakening for the North Atlantic (Renault et al. 2016c; 30%) but is more than the U.S. West Coast (no significant changes). The mean wind work is reduced by the current feedback only if the mean currents are strong enough, which is not the case for the U.S. West Coast (mean currents of less than 0.2 m s^{-1}). Consistently, the

weakening of the mean wind work slows down the mean circulation by 15% (against 27% for the North Atlantic). This furthermore locally reduces the barotropic conversion of energy from mean to eddy by 15%, weakening the EKE generation over Madagascar Channel and the Agulhas Basin region. As shown by, for example, Renault et al. (2016d), the current feedback induces a surface stress curl opposite to the current vorticity that deflects energy from the geostrophic current into the atmosphere and dampens eddies. It induces a mean pathway of energy from the ocean to the atmosphere over all the AC. As a result, the EKE is drastically reduced by 25% over the whole domain. The deflection of energy can be between 2 and 3 times larger over the Agulhas Basin region and

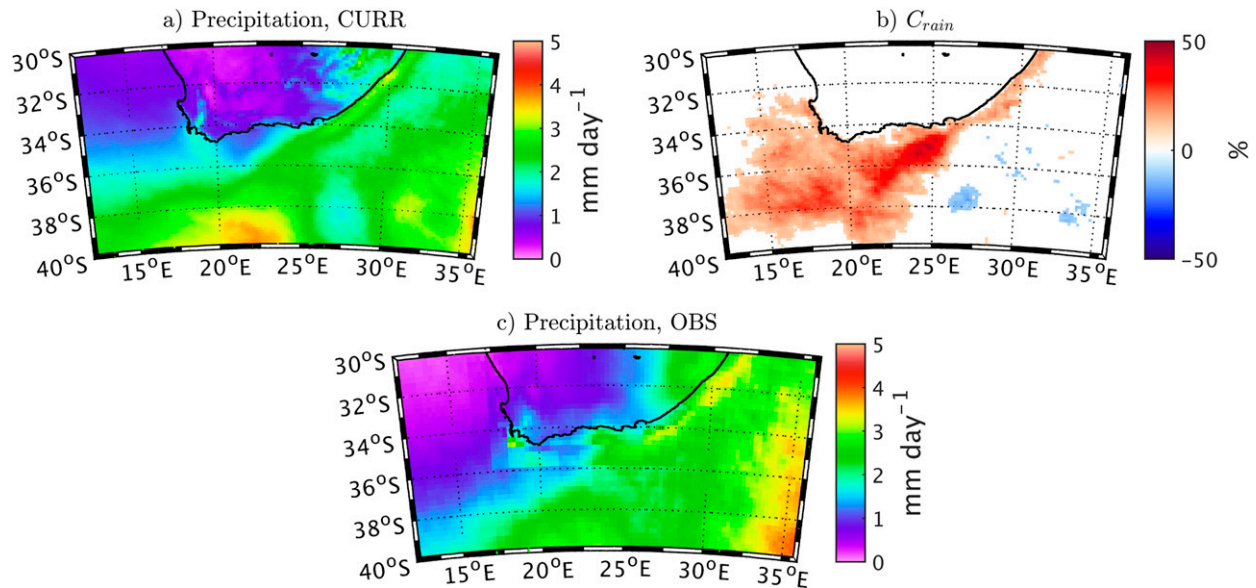


FIG. 14. Precipitation rate response to the current feedback. (a) Mean precipitation rate from CURR over the period 2000–04. (b) Relative difference C_{rain} (see text) between NOCURR and CURR. Only the significant values ($\sigma > 95\%$ using the Student's t test) are shown. (c) Mean precipitation rate from the Tropical Rainfall Measuring Mission (satellite data). The mean precipitation rate is realistically reproduced by CURR. The warmer sea surface temperature and associated larger SST gradients in CURR over the Agulhas Basin and the Benguela likely induce larger precipitation in CURR with respect to NOCURR.

the Gulf Stream compared to the U.S. West Coast (Renault et al. 2016d,c). There is a strong correlation between eddy wind work and EKE: the larger the EKE, the larger the sink of energy. Note that the mean wind work could be reduced further by including the full Indian Ocean Gyre in our domain. As shown by Luo et al. (2005) and Renault et al. (2016c), this could slow down the mean circulation, reduce the mean wind work and the generation of Natal pulses over the Madagascar Channel by barotropic conversion of energy from mean to eddy, and thus diminish furthermore the EKE.

An indirect effect of the current feedback is an improvement of the representation of the mean AC dynamic. Using the available observations, we show the AC retroflection can be classified in five regimes of variability: The two first regimes can be identified as central retroflection and a western retroflection. They represent 51% and 24% of the occurrences, respectively. The third category is another western retroflection. Finally, the fourth and fifth regimes are eastern retroflections (upstream retroflection) that are related to a large EKE near Port Elizabeth and likely to the Natal pulses. The simulation without current feedback (NOCURR) has a too frequent upstream retroflection because it overestimates the EKE and the presence of a standing eddy near Port Elizabeth. By dampening the eddy activity, the current feedback in CURR weakens the influence of the standing eddy on the retroflection, improving its representation.

We then evaluated the AC leakage using Lagrangian particles and the method developed by Rouault et al. (2009) and tested by van Sebille et al. (2010). By changing the AC dynamic, we show the current feedback increases the AC leakage by 21% from 10.6 to 12.9 Sv. We highlight a relationship between the EKE near Port Elizabeth and the leakage: a large EKE can induce a shortcut of the AC and thus a weakening of the AC leakage. The larger leakage in CURR, compared to NOCURR, modifies the water masses' characteristics of the western Agulhas Basin and of the Benguela region. It allows warmer SST (by 1.5° and 0.8°C, respectively) and saltier and warmer subsurface water. Finally, the mean offshore Agulhas rings corridor is altered by the current feedback. The shedding of the eddies is shifted northward, and, the Agulhas rings propagate less far north. This is consistent with McClean et al. (2011) and explains the improvement of the Agulhas rings properties in their simulation.

Consistently with previous studies, we show that the atmosphere responds to the surface current. A reduction of the surface stress allows the surface wind to accelerate; the effect can be felt up to 350 m. We further show the current–wind coupling coefficient s_w depends on the marine boundary layer height. An uncoupled simulation that estimates the surface stress using the wind relative to the surface current, but does not have a parameterization of the wind response to the current feedback, overestimates the dampening of the eddies and the

mean input of energy from the atmosphere to the ocean $F_m K_m$ and therefore the slowdown of the circulation. Following Renault et al. (2016d), in uncoupled oceanic simulations the surface stress should be estimated with a velocity that is the wind relative to the current corrected by the current–wind coupling coefficient s_w :

$$\mathbf{U} = \mathbf{U}_a - (1 - s_w)\mathbf{U}_o, \quad (10)$$

where \mathbf{U}_a and \mathbf{U}_o are the surface wind and the surface current, respectively. The parameterization suggested by Renault et al. (2016d) should be tested using different constant values of s_w estimated from coupled simulations but also for regions that present a large spread of s_w values, using a spatial- and temporal-dependent s_w . Such a parameterization should allow us to reproduce the partial reenergization of the ocean but also to simulate a realistic reduction of $F_m K_m$ and the associated slowdown of the circulation (as estimated from a coupled simulation). Dedicated studies should be done to assess what drives s_w and its likely dependence on the marine boundary layer parameterization in the atmospheric models. Global models with a not too coarse spatial resolution should be run for a long period to estimate s_w globally.

The main effect of the current feedback is a dampening of the eddy kinetic energy (EKE): it deflects energy from the ocean to the atmosphere. As shown by Gaube et al. (2015) and Renault et al. (2016d), it induces an additional Ekman pumping in the ocean that provides a mechanism for weakening an eddy. The SST feedback is potentially another important air–sea interaction. Seo et al. (2015) and Gaube et al. (2015) demonstrate the SST feedback can induce a comparable Ekman pumping velocity as the current feedback. However, it primarily affects the eddy propagation, with no effect on the amplitude. This is consistent with our results. The mean eddy wind work from NOCURR is roughly equal to zero, for example, over the Agulhas retroflection and the Agulhas Return Current. That means the thermal feedback does not induce a significant mean transfer of energy at eddy scale between the ocean to the atmosphere and does not directly affect the EKE. However, from NOCURR to CURR, a weakening of the SST front of the Agulhas ring in NOCURR may also partially explain the changes of the eddy corridor from NOCURR to CURR. To properly assess the SST feedback effect on the ocean, another coupled simulation should be integrated for a few years, yet, when coupling ROMS to WRF, a smoothed SST (i.e., without the mesoscale signal) should be sent to WRF by ROMS. Although this is not in the scope of this study, we aim to investigate it soon.

We show here that a high-resolution, coupled, ocean–atmosphere model with the current feedback improves the representation of oceanic current (both mean and mesoscale) and of the AC retroflection processes. A simulation without current feedback may have two important biases for the Benguela: 1) a poor representation of the AC leakage and consequently the water masses and biogeochemical materials and 2) an overestimation of the eddy life, intensity, quenching of nutrients, and offshore advection of biogeochemical materials (Gruber et al. 2011; Nagai et al. 2015; Renault et al. 2016a). To conclude, the AC leakage of Indian Ocean waters to the Atlantic is known to be a key process for the closure of the thermohaline circulation (de Ruijter et al. 1999b; Beal et al. 2011). Recently, Beal et al. (2011) show the AC leakage could strengthen the Atlantic meridional overturning circulation, counteracting its slowdown due to global warming and melting ice. A high-resolution, coupled, ocean–atmosphere model that takes into account the current feedback may be crucial for a realistic representation of the global thermohaline circulation.

Acknowledgments. We appreciate support from the Office of Naval Research (ONR N00014-12-1-0939), the National Science Foundation (OCE-1419450), the California Ocean Protection Council grant (Integrated Modeling Assessments and Projections for the California Current system), and the Bureau of Ocean Energy Management (Grant M14AC00021). This work used the Extreme Science and Engineering Discovery Environment (XSEDE) and Yellowstone (NCAR) computers. The authors are grateful to B. Blanke and N. Grima for making their ARIANE code available and for their support. The authors want to thank three anonymous reviewers for their comments as well as Sebastien Masson for useful discussions.

REFERENCES

- Backeberg, B. C., P. Penven, and M. Rouault, 2012: Impact of intensified Indian Ocean winds on mesoscale variability in the Agulhas system. *Nat. Climate Change*, **2**, 608–612, doi:10.1038/nclimate1587.
- Barnier, B., and Coauthors, 2006: Impact of partial steps and momentum advection schemes in a global ocean circulation model at eddy-permitting resolution. *Ocean Dyn.*, **56**, 543–567, doi:10.1007/s10236-006-0082-1.
- Beal, L. M., and S. Elipot, 2016: Broadening not strengthening of the Agulhas Current since the early 1990s. *Nature*, **540**, 570–573, doi:10.1038/nature19853.
- , and Coauthors, 2011: On the role of the Agulhas system in ocean circulation and climate. *Nature*, **472**, 429–436, doi:10.1038/nature09983.
- , S. Elipot, A. Houk, and G. M. Leber, 2015: Capturing the transport variability of a western boundary jet: Results from

- the Agulhas Current Time-Series Experiment (ACT). *J. Phys. Oceanogr.*, **45**, 1302–1324, doi:[10.1175/JPO-D-14-0119.1](https://doi.org/10.1175/JPO-D-14-0119.1).
- Bentamy, A., S. A. Grodsky, B. Chapron, and J. A. Carton, 2013: Compatibility of C- and Ku-band scatterometer winds: ERS-2 and QuikSCAT. *J. Mar. Syst.*, **117–118**, 72–80, doi:[10.1016/j.jmarsys.2013.02.008](https://doi.org/10.1016/j.jmarsys.2013.02.008).
- Biastoch, A., C. W. Böning, J. Getzlaff, J.-M. Molines, and G. Madec, 2008a: Causes of interannual-decadal variability in the meridional overturning circulation of the midlatitude North Atlantic Ocean. *J. Climate*, **21**, 6599–6615, doi:[10.1175/2008JCLI2404.1](https://doi.org/10.1175/2008JCLI2404.1).
- , —, and J. Lutjeharms, 2008b: Agulhas leakage dynamics affects decadal variability in Atlantic overturning circulation. *Nature*, **456**, 489–492, doi:[10.1038/nature07426](https://doi.org/10.1038/nature07426).
- , J. Lutjeharms, C. W. Böning, and M. Scheinert, 2008c: Mesoscale perturbations control inter-ocean exchange south of Africa. *Geophys. Res. Lett.*, **35**, L20602, doi:[10.1029/2008GL035132](https://doi.org/10.1029/2008GL035132).
- , L. Beal, J. Lutjeharms, and T. Casal, 2009: Variability and coherence of the Agulhas Undercurrent in a high-resolution ocean general circulation model. *J. Phys. Oceanogr.*, **39**, 2417–2435, doi:[10.1175/2009JPO4184.1](https://doi.org/10.1175/2009JPO4184.1).
- Blanke, B., M. Arhan, G. Madec, and S. Roche, 1999: Warm water paths in the equatorial Atlantic as diagnosed with a general circulation model. *J. Phys. Oceanogr.*, **29**, 2753–2768, doi:[10.1175/1520-0485\(1999\)029<2753:WWPITE>2.0.CO;2](https://doi.org/10.1175/1520-0485(1999)029<2753:WWPITE>2.0.CO;2).
- Boebel, O., C. Duncombe Rae, S. Garzoli, J. Lutjeharms, P. Richardson, T. Rossby, C. Schmid, and W. Zenk, 1998: Float experiment studies interocean exchanges at the tip of Africa. *Eos, Trans. Amer. Geophys. Union*, **79**, 1–8, doi:[10.1029/98EO00001](https://doi.org/10.1029/98EO00001).
- Capet, X., F. Colas, P. Penven, P. Marchesiello, and J. C. McWilliams, 2008a: Eddies in eastern boundary subtropical upwelling systems. *Ocean Modeling in an Eddying Regime*, *Geophys. Monogr.*, Vol. 177, Amer. Geophys. Union, 131–147, doi:[10.1029/177GM10](https://doi.org/10.1029/177GM10).
- , J. McWilliams, M. Molemaker, and A. Shchepetkin, 2008b: Mesoscale to submesoscale transition in the California Current system. Part I: Flow structure, eddy flux, and observational tests. *J. Phys. Oceanogr.*, **38**, 29–43, doi:[10.1175/2007JPO3671.1](https://doi.org/10.1175/2007JPO3671.1).
- Carton, J. A., and B. S. Giese, 2008: A reanalysis of ocean climate using Simple Ocean Data Assimilation (SODA). *Mon. Wea. Rev.*, **136**, 2999–3017, doi:[10.1175/2007MWR1978.1](https://doi.org/10.1175/2007MWR1978.1).
- Chelton, D. B., and M. G. Schlax, 2003: The accuracies of smoothed sea surface height fields constructed from tandem satellite altimeter datasets. *J. Atmos. Oceanic Technol.*, **20**, 1276–1302, doi:[10.1175/1520-0426\(2003\)020<1276:TAOSSS>2.0.CO;2](https://doi.org/10.1175/1520-0426(2003)020<1276:TAOSSS>2.0.CO;2).
- , —, M. H. Freilich, and R. F. Milliff, 2004: Satellite measurements reveal persistent small-scale features in ocean winds. *Science*, **303**, 978–983, doi:[10.1126/science.1091901](https://doi.org/10.1126/science.1091901).
- , —, and R. M. Samelson, 2007: Summertime coupling between sea surface temperature and wind stress in the California Current system. *J. Phys. Oceanogr.*, **37**, 495–517, doi:[10.1175/JPO3025.1](https://doi.org/10.1175/JPO3025.1).
- Chen, H., E. K. Schneider, and Z. Wu, 2016: Mechanisms of internally generated decadal-to-multidecadal variability of SST in the Atlantic Ocean in a coupled GCM. *Climate Dyn.*, **46**, 1517–1546, doi:[10.1007/s00382-015-2660-8](https://doi.org/10.1007/s00382-015-2660-8).
- Cornillon, P., and K. Park, 2001: Warm core ring velocities inferred from NSCAT. *Geophys. Res. Lett.*, **28**, 575–578, doi:[10.1029/2000GL011487](https://doi.org/10.1029/2000GL011487).
- Dawe, J. T., and L. Thompson, 2006: Effect of ocean surface currents on wind stress, heat flux, and wind power input to the ocean. *Geophys. Res. Lett.*, **33**, L09604, doi:[10.1029/2006GL025784](https://doi.org/10.1029/2006GL025784).
- Dawson, A., A. J. Matthews, D. P. Stevens, M. J. Roberts, and P. L. Vidale, 2013: Importance of oceanic resolution and mean state on the extra-tropical response to El Niño in a matrix of coupled models. *Climate Dyn.*, **41**, 1439–1452, doi:[10.1007/s00382-012-1518-6](https://doi.org/10.1007/s00382-012-1518-6).
- de Ruijter, W. P. M., A. Biastoch, S. Drijfhout, J. Lutjeharms, R. Matano, T. Pichevin, P. V. Leeuwen, and W. Weijer, 1999a: Indian-Atlantic interocean exchange: Dynamics, estimation and impact. *J. Geophys. Res.*, **104**, 20 885–20 910, doi:[10.1029/1998JC900099](https://doi.org/10.1029/1998JC900099).
- , P. J. van Leeuwen, and J. R. Lutjeharms, 1999b: Generation and evolution of Natal pulses: Solitary meanders in the Agulhas Current. *J. Phys. Oceanogr.*, **29**, 3043–3055, doi:[10.1175/1520-0485\(1999\)029<3043:GAEONP>2.0.CO;2](https://doi.org/10.1175/1520-0485(1999)029<3043:GAEONP>2.0.CO;2).
- Desbiolles, F., B. Blanke, A. Bentamy, and C. Roy, 2016: Response of the Southern Benguela upwelling system to fine-scale modifications of the coastal wind. *J. Mar. Syst.*, **156**, 46–55, doi:[10.1016/j.jmarsys.2015.12.002](https://doi.org/10.1016/j.jmarsys.2015.12.002).
- Dewar, W. K., and G. R. Flierl, 1987: Some effects of the wind on rings. *J. Phys. Oceanogr.*, **17**, 1653–1667, doi:[10.1175/1520-0485\(1987\)017<1653:SEOTWO>2.0.CO;2](https://doi.org/10.1175/1520-0485(1987)017<1653:SEOTWO>2.0.CO;2).
- Ducet, N., P.-Y. Le Traon, and G. Reverdin, 2000: Global high-resolution mapping of ocean circulation from TOPEX/Poseidon and ERS-1 and -2. *J. Geophys. Res.*, **105**, 19 477–19 498, doi:[10.1029/2000JC900063](https://doi.org/10.1029/2000JC900063).
- Duhaut, T. H., and D. N. Straub, 2006: Wind stress dependence on ocean surface velocity: Implications for mechanical energy input to ocean circulation. *J. Phys. Oceanogr.*, **36**, 202–211, doi:[10.1175/JPO2842.1](https://doi.org/10.1175/JPO2842.1).
- Eden, C., and H. Dietze, 2009: Effects of mesoscale eddy/wind interactions on biological new production and eddy kinetic energy. *J. Geophys. Res.*, **114**, C05023, doi:[10.1029/2008JC005129](https://doi.org/10.1029/2008JC005129).
- Fairall, C., E. F. Bradley, J. Hare, A. Grachev, and J. Edson, 2003: Bulk parameterization of air–sea fluxes: Updates and verification for the COARE algorithm. *J. Climate*, **16**, 571–591, doi:[10.1175/1520-0442\(2003\)016<0571:BPOASF>2.0.CO;2](https://doi.org/10.1175/1520-0442(2003)016<0571:BPOASF>2.0.CO;2).
- Freedman, D., and P. Diaconis, 1981: On the histogram as a density estimator: L 2 theory. *Z. Wahrscheinlichkeitstheorie Verw. Geb.*, **57**, 453–476.
- Gaube, P., D. B. Chelton, R. M. Samelson, M. G. Schlax, and L. W. O’Neill, 2015: Satellite observations of mesoscale eddy-induced Ekman pumping. *J. Phys. Oceanogr.*, **45**, 104–132, doi:[10.1175/JPO-D-14-0032.1](https://doi.org/10.1175/JPO-D-14-0032.1).
- Gordon, A. L., 2003: Oceanography: The browniest retroflection. *Nature*, **421**, 904–905, doi:[10.1038/421904a](https://doi.org/10.1038/421904a).
- , J. R. Lutjeharms, and M. L. Gründlingh, 1987: Stratification and circulation at the Agulhas retroflection. *Deep-Sea Res.*, **34A**, 565–599, doi:[10.1016/0198-0149\(87\)90006-9](https://doi.org/10.1016/0198-0149(87)90006-9).
- Gruber, N., Z. Lachkar, H. Frenzel, P. Marchesiello, M. Münnich, J. C. McWilliams, T. Nagai, and G.-K. Plattner, 2011: Eddy-induced reduction of biological production in eastern boundary upwelling systems. *Nat. Geosci.*, **4**, 787–792, doi:[10.1038/ngeo1273](https://doi.org/10.1038/ngeo1273).
- Halo, I., B. Backeberg, P. Penven, I. Anson, C. Reason, and J. Ullgren, 2014: Eddy properties in the Mozambique Channel: A comparison between observations and two numerical ocean circulation models. *Deep-Sea Res. II*, **100**, 38–53, doi:[10.1016/j.dsr2.2013.10.015](https://doi.org/10.1016/j.dsr2.2013.10.015).

- Harris, I., P. Jones, T. Osborn, and D. Lister, 2014: Updated high-resolution grids of monthly climatic observations—The CRU TS3.10 dataset. *Int. J. Climatol.*, **34**, 623–642, doi:10.1002/joc.3711.
- Harris, T. F. W., R. Legeckis, and D. Van Forest, 1978: Satellite infra-red images in the Agulhas Current system. *Deep-Sea Res.*, **25**, 543–548, doi:10.1016/0146-6291(78)90642-2.
- Huffman, G. J., and Coauthors, 2007: The TRMM Multisatellite Precipitation Analysis (TMPA): Quasi-global, multiyear, combined-sensor precipitation estimates at fine scales. *J. Hydrometeorol.*, **8**, 38–55, doi:10.1175/JHM560.1.
- Hughes, C. W., and C. Wilson, 2008: Wind work on the geostrophic ocean circulation: An observational study of the effect of small scales in the wind stress. *J. Geophys. Res.*, **113**, C02016, doi:10.1029/2007JC004371.
- Kilpatrick, T., N. Schneider, and B. Qiu, 2016: Atmospheric response to a midlatitude SST front: Alongfront winds. *J. Atmos. Sci.*, **73**, 3489–3509, doi:10.1175/JAS-D-15-0312.1.
- Large, W. G., J. C. McWilliams, and S. C. Doney, 1994: Oceanic vertical mixing: A review and a model with a nonlocal boundary layer parameterization. *Rev. Geophys.*, **32**, 363–404, doi:10.1029/94RG01872.
- Lemarié, F., J. Kurian, A. F. Shchepetkin, M. J. Molemaker, F. Colas, and J. C. McWilliams, 2012: Are there inescapable issues prohibiting the use of terrain-following coordinates in climate models? *Ocean Modell.*, **42**, 57–79, doi:10.1016/j.ocemod.2011.11.007.
- Le Traon, P., F. Nadal, and N. Ducet, 1998: An improved mapping method of multisatellite altimeter data. *J. Atmos. Oceanic Technol.*, **15**, 522–534, doi:10.1175/1520-0426(1998)015<0522:AIMMOM>2.0.CO;2.
- Liu, W. T., X. Xie, and P. P. Niiler, 2007: Ocean–atmosphere interaction over Agulhas extension meanders. *J. Climate*, **20**, 5784–5797, doi:10.1175/2007JCLI1732.1.
- Loveday, B. R., J. V. Durgadoo, C. J. Reason, A. Biastoch, and P. Penven, 2014: Decoupling of the Agulhas leakage from the Agulhas Current. *J. Phys. Oceanogr.*, **44**, 1776–1797, doi:10.1175/JPO-D-13-093.1.
- Luo, J.-J., S. Masson, E. Roeckner, G. Madec, and T. Yamagata, 2005: Reducing climatology bias in an ocean–atmosphere CGCM with improved coupling physics. *J. Climate*, **18**, 2344–2360, doi:10.1175/JCLI3404.1.
- Lutjeharms, J. R. E., 2006: *The Agulhas Current*. Springer-Verlag, 329 pp.
- , and R. Van Ballegooyen, 1988a: Anomalous upstream retroreflection in the Agulhas Current. *Science*, **240**, 1770, doi:10.1126/science.240.4860.1770.
- , and —, 1988b: The retroreflection of the Agulhas Current. *J. Phys. Oceanogr.*, **18**, 1570–1583, doi:10.1175/1520-0485(1988)018<1570:TROTAC>2.0.CO;2.
- , and D. Webb, 1995: Modelling the Agulhas Current system with FRAM (Fine Resolution Antarctic Model). *Deep-Sea Res. I*, **42**, 523–551, doi:10.1016/0967-0637(94)00031-M.
- Lynch, S., 2004: Development of a raster database of annual, monthly and daily rainfall for southern Africa: Report to the Water Research Commission. Water Research Commission Rep., 78 pp.
- Maltrud, M. E., and J. L. McClean, 2005: An eddy resolving global $1/10^\circ$ ocean simulation. *Ocean Modell.*, **8**, 31–54, doi:10.1016/j.ocemod.2003.12.001.
- Matano, R., and E. Beier, 2003: A kinematic analysis of the Indian/Atlantic interocean exchange. *Deep-Sea Res. II*, **50**, 229–249, doi:10.1016/S0967-0645(02)00395-8.
- McClean, J. L., and Coauthors, 2011: A prototype two-decade fully-coupled fine-resolution CCSM simulation. *Ocean Modell.*, **39**, 10–30, doi:10.1016/j.ocemod.2011.02.011.
- McWilliams, J. C., 1985: Submesoscale, coherent vortices in the ocean. *Rev. Geophys.*, **23**, 165–182, doi:10.1029/RG023i002p00165.
- Minobe, S., A. Kuwano-Yoshida, N. Komori, S.-P. Xie, and R. J. Small, 2008: Influence of the Gulf Stream on the troposphere. *Nature*, **452**, 206–209, doi:10.1038/nature06690.
- Nagai, T., N. Gruber, H. Frenzel, Z. Lachkar, J. C. McWilliams, and G.-K. Plattner, 2015: Dominant role of eddies and filaments in the offshore transport of carbon and nutrients in the California Current system. *J. Geophys. Res. Oceans*, **120**, 5318–5341, doi:10.1002/2015JC010889.
- Pacanowski, R., 1987: Effect of equatorial currents on surface stress. *J. Phys. Oceanogr.*, **17**, 833–838, doi:10.1175/1520-0485(1987)017<0833:EOECOS>2.0.CO;2.
- Park, H., D. Lee, W.-P. Jeon, S. Hahn, J. Kim, J. Kim, J. Choi, and H. Choi, 2006: Drag reduction in flow over a two-dimensional bluff body with a blunt trailing edge using a new passive device. *J. Fluid Mech.*, **563**, 389–414, doi:10.1017/S0022112006001364.
- Penven, P., 2000: A numerical study of the southern Benguela circulation with an application to fish recruitment. Ph.D. dissertation, Université de Bretagne Occidentale, 141 pp.
- , J. Lutjeharms, and P. Florenchie, 2006: Madagascar: A pacemaker for the Agulhas Current system? *Geophys. Res. Lett.*, **33**, L17609, doi:10.1029/2006GL026854.
- Putrasahan, D., L. M. Beal, B. P. Kirtman, and Y. Cheng, 2015: A new Eulerian method to estimate spicy Agulhas leakage in climate models. *Geophys. Res. Lett.*, **42**, 4532–4539, doi:10.1002/2015GL064482.
- , B. P. Kirtman, and L. M. Beal, 2016: Modulation of SST interannual variability in Agulhas leakage region associated with ENSO. *J. Climate*, **29**, 7089–7102, doi:10.1175/JCLI-D-15-0172.1.
- Rae, C. D., F. Shillington, J. Agenbag, J. Taunton-Clark, and M. Gründlingh, 1992: An Agulhas ring in the South Atlantic Ocean and its interaction with the Benguela upwelling frontal system. *Deep-Sea Res.*, **39A**, 2009–2027, doi:10.1016/0198-0149(92)90011-H.
- Renault, L., B. Dewitte, M. Falvey, R. Garreaud, V. Echevin, and F. Bonjean, 2009: Impact of atmospheric coastal jet off central Chile on sea surface temperature from satellite observations (2000–2007). *J. Geophys. Res.*, **114**, C08006, doi:10.1029/2008JC005083.
- , and Coauthors, 2012: Upwelling response to atmospheric coastal jets off central Chile: A modeling study of the October 2000 event. *J. Geophys. Res.*, **117**, C02030, doi:10.1029/2011JC007446.
- , C. Deutsch, J. C. McWilliams, H. Frenzel, J.-H. Liang, and F. Colas, 2016a: Partial decoupling of primary productivity from upwelling in the California Current system. *Nat. Geosci.*, **9**, 505–508, doi:10.1038/ngeo2722.
- , A. Hall, and J. C. McWilliams, 2016b: Orographic shaping of U.S. West Coast wind profiles during the upwelling season. *Climate Dyn.*, **46**, 273–289, doi:10.1007/s00382-015-2583-4.
- , M. J. Molemaker, J. Gula, S. Masson, and J. C. McWilliams, 2016c: Control and stabilization of the Gulf Stream by oceanic current interaction with the atmosphere. *J. Phys. Oceanogr.*, **46**, 3439–3453, doi:10.1175/JPO-D-16-0115.1.
- , —, J. C. McWilliams, A. F. Shchepetkin, F. Lemarié, D. Chelton, S. Illig, and A. Hall, 2016d: Modulation of wind work by oceanic current interaction with the

- atmosphere. *J. Phys. Oceanogr.*, **46**, 1685–1704, doi:[10.1175/JPO-D-15-0232.1](https://doi.org/10.1175/JPO-D-15-0232.1).
- Richardson, P. L., 2007: Agulhas leakage into the Atlantic estimated with subsurface floats and surface drifters. *Deep-Sea Res. I*, **54**, 1361–1389, doi:[10.1016/j.dsr.2007.04.010](https://doi.org/10.1016/j.dsr.2007.04.010).
- Rio, M., S. Guinehut, and G. Larnicol, 2011: New CNES-CLS09 global mean dynamic topography computed from the combination of GRACE data, altimetry, and in situ measurements. *J. Geophys. Res.*, **116**, C07018, doi:[10.1029/2010JC006505](https://doi.org/10.1029/2010JC006505).
- , S. Mulet, and N. Picot, 2013: New global Mean Dynamic Topography from a GOCE geoid model, altimeter measurements and oceanographic in-situ data. *Proc. ESA Living Planet Symp. 2013*, Edinburgh, United Kingdom, ESA, ESA SP-722. [Available online at https://ftp.space.dtu.dk/pub/loana/papers/s211_2rio.pdf.]
- Risien, C. M., and D. B. Chelton, 2008: A global climatology of surface wind and wind stress fields from eight years of QuikSCAT scatterometer data. *J. Phys. Oceanogr.*, **38**, 2379–2413, doi:[10.1175/2008JPO3881.1](https://doi.org/10.1175/2008JPO3881.1).
- Rouault, M., and P. Penven, 2011: New perspectives on Natal pulses from satellite observations. *J. Geophys. Res.*, **116**, C07013, doi:[10.1029/2010JC006866](https://doi.org/10.1029/2010JC006866).
- , —, and B. Pohl, 2009: Warming in the Agulhas Current system since the 1980's. *Geophys. Res. Lett.*, **36**, L12602, doi:[10.1029/2009GL037987](https://doi.org/10.1029/2009GL037987).
- Saha, S., and Coauthors, 2010: The NCEP Climate Forecast System Reanalysis. *Bull. Amer. Meteor. Soc.*, **91**, 1015–1057, doi:[10.1175/2010BAMS3001.1](https://doi.org/10.1175/2010BAMS3001.1).
- Schouten, M. W., W. P. de Ruijter, and P. J. van Leeuwen, 2002: Upstream control of Agulhas ring shedding. *J. Geophys. Res.*, **107**, doi:[10.1029/2001JC000804](https://doi.org/10.1029/2001JC000804).
- Scott, R. B., and Y. Xu, 2009: An update on the wind power input to the surface geostrophic flow of the World Ocean. *Deep-Sea Res. I*, **56**, 295–304, doi:[10.1016/j.dsr.2008.09.010](https://doi.org/10.1016/j.dsr.2008.09.010).
- Seo, H., A. J. Miller, and J. R. Norris, 2015: Eddy-wind interaction in the California Current system: Dynamics and impacts. *J. Phys. Oceanogr.*, **46**, 439–459, doi:[10.1175/JPO-D-15-0086.1](https://doi.org/10.1175/JPO-D-15-0086.1).
- Shchepetkin, A. F., 2015: An adaptive, Courant-number-dependent implicit scheme for vertical advection in oceanic modeling. *Ocean Modell.*, **91**, 38–69, doi:[10.1016/j.ocemod.2015.03.006](https://doi.org/10.1016/j.ocemod.2015.03.006).
- , and J. C. McWilliams, 2005: The Regional Oceanic Modeling System (ROMS): A split-explicit, free-surface, topography-following-coordinate oceanic model. *Ocean Modell.*, **9**, 347–404, doi:[10.1016/j.ocemod.2004.08.002](https://doi.org/10.1016/j.ocemod.2004.08.002).
- Skamarock, W. C., and Coauthors, 2008: A description of the Advanced Research WRF version 3. NCAR Tech. Note NCAR/TN-475+STR, 113 pp., doi:[10.5065/D68S4MVH](https://doi.org/10.5065/D68S4MVH).
- Smagorinsky, J., 1963: General circulation experiments with the primitive equations: I. The basic experiment. *Mon. Wea. Rev.*, **91**, 99–164, doi:[10.1175/1520-0493\(1963\)091<0099:GCEWTP>2.3.CO;2](https://doi.org/10.1175/1520-0493(1963)091<0099:GCEWTP>2.3.CO;2).
- Small, R. J., and Coauthors, 2008: Air–sea interaction over ocean fronts and eddies. *Dyn. Atmos. Oceans*, **45**, 274–319, doi:[10.1016/j.dynatmoce.2008.01.001](https://doi.org/10.1016/j.dynatmoce.2008.01.001).
- Spall, M. A., 2007: Midlatitude wind stress–sea surface temperature coupling in the vicinity of oceanic fronts. *J. Climate*, **20**, 3785–3801, doi:[10.1175/JCLI4234.1](https://doi.org/10.1175/JCLI4234.1).
- Stern, M. E., 1975: *Ocean Circulation Physics*. Academic Press, 246 pp.
- Thoppil, P. G., J. G. Richman, and P. J. Hogan, 2011: Energetics of a global ocean circulation model compared to observations. *Geophys. Res. Lett.*, **38**, L15607, doi:[10.1029/2011GL048347](https://doi.org/10.1029/2011GL048347).
- Valcke, S., 2013: The OASIS3 coupler: A European climate modelling community software. *Geosci. Model Dev.*, **6**, 373–388, doi:[10.5194/gmd-6-373-2013](https://doi.org/10.5194/gmd-6-373-2013).
- van Leeuwen, P. J., W. P. de Ruijter, and J. R. Lutjeharms, 2000: Natal pulses and the formation of Agulhas rings. *J. Geophys. Res.*, **105**, 6425–6436, doi:[10.1029/1999JC900196](https://doi.org/10.1029/1999JC900196).
- van Sebille, E., C. N. Barron, A. Biastoch, P. J. van Leeuwen, F. C. Vossepoel, and W. de Ruijter, 2009: Relating Agulhas leakage to the Agulhas Current retroflection location. *Ocean Sci.*, **5**, 511–521, doi:[10.5194/os-5-511-2009](https://doi.org/10.5194/os-5-511-2009).
- , P. J. Van Leeuwen, A. Biastoch, and W. P. de Ruijter, 2010: Flux comparison of Eulerian and Lagrangian estimates of Agulhas leakage: A case study using a numerical model. *Deep-Sea Res. I*, **57**, 319–327, doi:[10.1016/j.dsr.2009.12.006](https://doi.org/10.1016/j.dsr.2009.12.006).
- Veitch, J., P. Penven, and F. Shillington, 2010: Modeling equilibrium dynamics of the Benguela Current system. *J. Phys. Oceanogr.*, **40**, 1942–1964, doi:[10.1175/2010JPO4382.1](https://doi.org/10.1175/2010JPO4382.1).
- von Storch, J.-S., H. Sasaki, and J. Marotzke, 2007: Wind-generated power input to the deep ocean: An estimate using a 1/10° general circulation model. *J. Phys. Oceanogr.*, **37**, 657–672, doi:[10.1175/JPO3001.1](https://doi.org/10.1175/JPO3001.1).
- Weijer, W., W. P. de Ruijter, H. A. Dijkstra, and P. J. van Leeuwen, 1999: Impact of interbasin exchange on the Atlantic overturning circulation. *J. Phys. Oceanogr.*, **29**, 2266–2284, doi:[10.1175/1520-0485\(1999\)029<2266:IOIEOT>2.0.CO;2](https://doi.org/10.1175/1520-0485(1999)029<2266:IOIEOT>2.0.CO;2).
- Wunsch, C., 1998: The work done by the wind on the oceanic general circulation. *J. Phys. Oceanogr.*, **28**, 2332–2340, doi:[10.1175/1520-0485\(1998\)028<2332:TWDBTW>2.0.CO;2](https://doi.org/10.1175/1520-0485(1998)028<2332:TWDBTW>2.0.CO;2).
- Xu, C., X. Zhai, and X.-D. Shang, 2016: Work done by atmospheric winds on mesoscale ocean eddies. *Geophys. Res. Lett.*, **43**, 12 174–12 180, doi:[10.1002/2016GL071275](https://doi.org/10.1002/2016GL071275).
- Zahn, R., 2009: Climate change: Beyond the CO2 connection. *Nature*, **460**, 335–336, doi:[10.1038/460335a](https://doi.org/10.1038/460335a).